PROGRESSIVE STRUCTURAL DEFECTS IN CANINE CENTRONUCLEAR MYOPATHY INDICATE A ROLE FOR HACD1 IN MAINTAINING SKELETAL MUSCLE MEMBRANE SYSTEMS

Gemma L. Walmsley[1]*, Stéphane Blot[2,3], Kerrie Venner[4], Caroline Sewry[5], Jocelyn Laporte[6], Jordan Blondelle[2,3], Inès Barthélémy[2,3], Marie Maurer[2,3], Nicolas Blanchard-Gutton[2,3], Fanny Pilot-Storck[2,3], Laurent Tiret[2,3] and Richard J. Piercy[1]

1: Comparative Neuromuscular Diseases Laboratory, Department of Clinical Sciences and Services, Royal Veterinary College, Royal College Street, London, NW1 0TU, United Kingdom

2: Inserm, IMRB U955-E10 Biology of the neuromuscular system, 8 rue du général Sarrail, 94000 Créteil, France

3: Université Paris-Est, École nationale vétérinaire d'Alfort (EnvA), 7 avenue du général de Gaulle, 94700 Maisons-Alfort, France

4 : Electron Microscopy Unit, Institute of Neurology, Queen Square House, Queen Square, London, WC1N 3BG, United Kingdom

5: Dubowitz Neuromuscular Centre, UCL Institute of Child Health and Great Ormond Street Hospital, 30 Guilford Street, London, WC1N 1EH, United Kingdom

6: Department of Translational Medicine and Neurogenetics, Institut de Genetique et de Biologie Moleculaire et Cellulaire (IGBMC), Inserm U964, CNRS UMR7104, Strasbourg University, 1 rue Laurent Fries, BP10142, 67404 Illkirch, France

***Corresponding author:** current address: Musculoskeletal Biology I, Institute of Ageing and Chronic Disease, University of Liverpool, William Henry Duncan Building, 6 West Derby Street, Liverpool, L7 8TX. Telephone: 0151 794 9309 Fax: 0151 706 5802 Email: glw22@liv.ac.uk.

Running title: Membrane defects in HACD1-deficient myopathy

Key words: muscle; centronuclear myopathy; myotubular myopathy; HACD1/PTPLA; dog model; membrane trafficking; very long chain fatty acid; t-tubule

Length of article: 17 text pages, 7 figures, 1 table

Supplemental material: 5 figures, 1 table

Funding: This work was supported by a project grant from The Myotubular Trust to RJP and via a studentship to GLW and RJP from the Biotechnology and Biological Sciences Research Council (BBSRC) (United Kingdom) (BB/F016891/1), additional funding was awarded to LT and SB by the Agence Nationale de la Recherche (ANR-12-JSV1-0005), the Association Française contre les Myopathies (14577, 15882, 16143 and 17124), the CNM Project and the Alliance program (22866ZM/10.020). The authors declare no conflict of interest.

Disclosures: None declared

Abstract

Mutations in hydroxyacyl-coA dehydratase 1 (*HACD1/PTPLA)* cause recessive congenital myopathies in humans and dogs. Hydroxyacyl-coA dehydratases are required for elongation of very long chain fatty acids and HACD1 has a role in early myogenesis but the functions of this striated muscle-specific enzyme in more differentiated skeletal muscle remain unknown. Canine HACD1-deficiency is histopathologically classified as a centronuclear myopathy (CNM): we investigated the hypothesis that muscle from HACD1-deficient dogs has membrane abnormalities in common with CNMs with different genetic causes. We demonstrate progressive changes in tubuloreticular and sarcolemmal membranes and mislocalized triads and mitochondria in skeletal muscle from animals deficient in HACD1. Further, comparable membranous abnormalities in cultured HACD1-deficient myotubes provide additional evidence that these defects are a primary consequence of altered HACD1 expression.

Our novel findings, including t-tubule dilatation and disorganization, associated with defects in this additional CNM-associated gene provide a definitive pathophysiological link with these disorders, confirm that dogs deficient in HACD1 are relevant models and strengthen the evidence for a unifying pathogenesis in CNMs via defective membrane trafficking and excitation-contraction coupling in muscle. These results build on previous work by determining further functional roles of HACD1 in muscle and provide new insight into the pathology and pathogenetic mechanisms of HACD1-CNM. Consequently, alterations in membrane properties associated with *HACD1* mutations should be investigated in humans with related phenotypes.

Introduction

Centronuclear myopathies (CNM) are a genetically heterogeneous group of congenital myopathies characterized clinically by paresis and skeletal muscle atrophy and histologically by abnormal centralization of myonuclei[1,2]. Genes classically associated with human centronuclear myopathies (CNMs) produce proteins involved in membrane trafficking or excitation-contraction coupling[3]. Principally, these include mutations in myotubularin (*MTM1*), a phosphoinositide phosphatase[4], amphiphysin 2 (*BIN1*), which promotes and senses membrane curvature[5], dynamin 2 (*DNM2*), a protein involved in membrane tubulation and fission[6] and the skeletal muscle ryanodine receptor (*RYR1*), the sarcoplasmic reticulum (SR) calcium release channel[7]. Other human CNMs are associated with mutations in *CCDC78*[8], *SPEG*[9], and *TTN*[10].

T-tubules are complex skeletal muscle membrane systems that conduct action potentials deep within the myofiber and into close proximity with the internal sarcoplasmic stores at the calcium release unit or triad. Several causative genes for CNM produce proteins that associate with t-tubules hence the severe weakness that occurs in CNMs might result from altered morphology of t-tubule or sarcoplasmic reticulum membranes, altered coupling between the voltage-gated DHPR and RyR1 calcium release channel, or more direct effects on RyR1 function or expression[11-22]. Additional membrane defects at the sarcolemma, myofiber hypotrophy and mislocalization of other proteins involved in membrane repair and recycling all strengthen the case for a more generalized derangement of membrane trafficking pathways in CNMs[14,18,19,21,23].

Canine HACD1-CNM, an autosomal recessive condition that was recognized in Labrador Retrievers 40 years ago, is the most common inherited myopathy in the breed[24-26]. A colony of affected dogs was established in France in 1992 enabling more detailed evaluation and the condition is now widely accepted as a CNM based on numerous clinical and pathological features in common with CNMs in humans[25,27-29]. Affected dogs do not develop myotatic reflexes and display markedly reduced muscle mass, hypotonia and paresis in comparison with littermates from 1 month of age. Clinical signs are initially progressive, but can stabilize at around 1 year of age[27-30]. Their muscle exhibits several characteristic and progressive features: an early and marked heterogeneity in fiber size with altered oxidative staining, then type 1 myofiber predominance followed by centralization of nuclei and fibrosis[27,28,31]. Linkage analysis implicated a short interspersed nuclear element (SINE) insertion in the protein tyrosine phosphatase-like, member A (*PTPLA*) gene (recently renamed hydroxyacyl-CoA dehydratase 1 (*HACD1*)) as the causative mutation that alters splicing and reduces expression of normal transcripts[29]. These include a full length, muscle-specific isoform named HACD1-fl (hereafter, for simplicity, termed HACD1) and a shorter, ubiquitous isoform named HACD1-

d5[29].

Recently, HACD1 enzyme deficiency was also implicated in a novel human autosomal recessive, congenital myopathy in an extended, consanguineous Bedouin family[32]. *HACD1* is highly expressed in developing and mature striated muscles[33-35] and encodes a 3-hydroxyacyl-CoA dehydratase enzyme with a role in very long chain fatty acid (VLCFA) biosynthesis, as part of the endoplasmic reticulum-bound, elongase complex[34,36,37]. VLCFA are metabolized in muscle as energy sources, but more importantly, are constituents of various membrane lipids, including phospholipids and sphingolipids, which have essential roles in membrane structure, fluidity, intracellular signaling and membrane trafficking[38,39]. *In vitro*, HACD1-deficient myoblasts have impaired myogenesis[35,40] and more specifically, defective myoblast fusion, likely due to altered sarcolemmal lipid content[40]. In yeast and plants, HACD1 homologues (Phs1 and PASTICCINO2 respectively) are essential for growth and development[37,41,42].

Here we investigate the hypothesis that canine HACD1-CNM recapitulates prominent features previously found in related human myopathies and have documented common findings of tubuloreticular disorganization and more general membrane abnormalities combined with mislocalization of other CNM proteins. Our work strengthens the evidence for a common pathogenesis between this myopathy and human CNMs, validates HACD1-CNM in dogs as a CNM model and reveals a previously unidentified role for HACD1 in muscle. Documenting pathological consequences associated with HACD1-deficiency in CNM provides further insight into CNM pathogenesis, confirms a general regulatory role for HACD1 in membrane composition and dynamics and specifically, in t-tubule/SR membrane maintenance in differentiated muscle.

Materials and methods

Dogs and sample collection

Homozygote (affected) (n = 5) and heterozygote (clinically normal) (n = 2) Labrador Retrievers (genotyped according to Pelé *et al.*[29]), in addition to normal Golden Retrievers (n = 2), were selected at the École nationale vétérinaire d'Alfort (Maisons-Alfort, France). Experiments on dogs were approved by the Anses/EnvA/Upec Ethics Committee (C2EA – 16; approval number 20/12/12-18) and all care and manipulations were performed in accordance with national and European legislation on animal experimentation. Clinical severity varied slightly between affected dogs, but all displayed characteristic signs of paresis, reduction in muscle mass and absent myotatic reflexes typical of the disease[25-29]. Previous work had determined the progression of general pathological features in a severely affected muscle, the biceps

femoris, therefore this muscle was selected for further evaluation by light and electron microscopy. Biopsy samples were obtained in a standard manner from dogs under general anaesthesia[28,29]; to evaluate temporal progression, dogs from a single litter were biopsied twice (from alternate sides) at two ages chosen in order to give a good representation of pathological features (at 11 months old, during the initial progressive stage of the disease, and again at 30 months of age when dogs would likely have advanced pathological features). Additional control samples were obtained from normal Beagle dogs (n = 4) kept in research colonies within the UK immediately following their euthanasia (for reasons unrelated to this study). Details of all dogs used in this work are summarized in supplemental table S1.

Muscle histology

Routine histological and histochemical stains were used to examine the pathological features in a subset of samples to confirm they were representative[25,27]. Canine muscle biopsy samples and additional test and control samples were first orientated for sectioning on corks with optimum cooling temperature mountant (Tissue-Tek OCT, Sakura Finetek UK Ltd, Thatcham, UK) and frozen in liquid nitrogen-cooled isopentane[26,28]. Cryosections (10 μm thickness) from dogs detailed in supplemental table S1 were stained with a panel of standard histological stains: haematoxylin and eosin (H&E), modified Gomori trichrome, nicotinamide adenine dinucleotide hydride (NADH-TR), succinate dehydrogenase (SDH), cytochrome oxidase (COX), oil red O and acid phosphatase. The oxidative staining pattern was evaluated using mitochondria-specific stains (COX and SDH) in addition to NADH-TR, which also stains SR[1]. The proportion of centrally-nucleated fibers (from a total of ≥500 fibers per dog taken over at least two fields of view) was determined from randomly-acquired images obtained using the 10x magnification objective from H&E stained cryosections using the ImageJ cell counter tool (ImageJ 1.45g, W.S. Rasband, National Institutes of Health, Bethesda, MD, 1997-2016; *http://rsb.info.nih.gov/ij* last accessed 26/09/2016). Pathological abnormalities were assessed (observer blinded to genotype) by subjective scoring (performed on H&E, Gomori trichrome and COX, SDH and NADH-TR oxidative enzyme stains) and objective counts of myofibers were performed from randomly acquired images (obtained using the 20x objective) of SDH-stained sections (minimum 250 fibers per dog taken over ≥3 fields of view; table 1).

Immunohistochemical staining

Immunohistochemistry was performed using a selection of antibodies to triad, membrane, cytoskeletal and myofibrillar proteins based on prominent ultrastructural features (see below) and human CNMs.

Use of each new antibody, fixation and permeabilization protocols were optimized on trial sections in parallel with control human muscle sections and additional canine disease controls (not shown)[43]. Immunohistochemistry was performed by incubating cryosections with each primary antibody in a humidified chamber for 1 hour at room temperature, after rinsing in copious amounts of phosphate buffered saline (PBS), species-appropriate secondary antibodies (goat anti-mouse IgG conjugated to Alexafluor 488, goat anti-mouse IgG conjugated to Alexafluor 594 and goat anti-rabbit IgG conjugated to Alexafluor 594 (Invitrogen, Fisher Scientific UK Ltd, Loughborough, UK)) were applied at 1:1000 in PBS for 1 hour at room temperature in a light-proof humidified chamber. Primary antibodies used were mouse monoclonal antibodies, unless otherwise stated: RyR1 (34C (Abcam, Cambridge, UK) 1:100), DHPR (1A (Affinity bioreagents, Fisher Scientific UK Ltd) 1:100), SERCA2 (IID8 (Affinity bioreagents) 1:500), dysferlin (1/7B6 (Leica Novocastra; Leica Biosystems, Milton Keynes, UK) 1:25), caveolin 3 (26 (Becton Dickinson, Oxford, UK) 1:200), desmin (D33 (Dako UK Ltd, Ely, UK) 1:100), sarcomeric myosin (MF20 (Developmental Studies Hybridoma Bank, Iowa City, IA) 1:50), developmental myosin heavy chain (RNMy2/9D2 (Leica Novocastra) 1:20), dystrophin (Dys2 (Leica Novocastra) 1:20), rabbit polyclonal antibody against BIN1-iso8 (R2406[21] 1:600). To obtain double labelling with multiple mouse monoclonal antibodies for evaluation of RyR1 (labeled with Alexafluor 594) with DHPR and SERCA2 (labeled with Alexafluor 488), Zenon™ antibody labels were employed according to the manufacturer's instructions (Invitrogen, Fisher Scientific UK Ltd).

Images were obtained using standardized exposures on a Leica DMRA2 wide field fluorescent microscope (Leica Microsystems, Sunnyvale, CA) equipped with an AxioCam MRm monochrome camera controlled via Axiovision software (version 4.8.2; Carl Zeiss Ltd., Cambridge, UK). Confocal fluorescence microscopy images were captured using a Leica SP5 confocal laser-scanning microscope using Argon (488), HeNe (594) and Diode (405) lasers.

Electron microscopy

Each muscle sample was kept chilled until placed in fixative within 10 minutes of biopsy. The entire sample (approximately 4 cm long and 1 cm diameter) was initially placed into 4% glutaraldehyde in 0.1M cacodylate buffer (pH 7.2) (Agar Scientific, Stanstead, UK) whilst clamped (to preserve myofiber length). The sample was then dissected further whilst in fixative (typically within 10 minutes) to produce small blocks (1-2 x 2-4mm) oriented with the long axis running along the myofibers; these samples then remained in fixative for 2 hours at room temperature. Samples were then rinsed in a

single wash of 0.1M cacodylate buffer and stored at 4°C until further processing. Subsequently, samples were processed in a standard manner using a mechanical tissue processor (Lynx EL EM Microscopy Tissue Processor, Reichert Jung, Ametek, Munich, Germany). Tissue was rinsed in 0.1M cacodylate buffer, post-fixed in 1% osmium tetroxide (Agar Scientific) for 2 hours at 4°C, dehydrated through graded ethanols and propylene oxide and embedded in Araldite resin (Agar Scientific) for both transverse and longitudinal sectioning. Blocks were prepared and semi-thin sections (500-800 nm) cut and stained with toluidine blue (1% saturated with borax, TAAB Laboratories Equipment Ltd, Aldermaston, UK) to select blocks in the desired orientation. Ultra-thin sections (approximately 65 nm thickness) were prepared from each dog. Sections for imaging were stained with saturated methanolic uranyl acetate and Reynold's lead citrate and examined on a CM10 transmission electron microscope (Philips, FEI UK Ltd, Cambridge, UK). Images were obtained using a Kodak Megaview III camera (SIS GmbH; Munster, Germany).

T-tubule morphometry: imaging, measurement and statistical analysis

T-tubules were evaluated morphometrically from electron micrographs to provide quantitative, objective data. Images used for t-tubule measurements were captured from longitudinal sections at 21,000x magnification in an identical manner for all samples. Evaluations of shape and size were performed for >120 t-tubules per dog from a minimum of five myofibers (table S1). T-tubules in the images were circumscribed using a pen tablet (intuos4, Wacom Europe GmbH, Krefeld, Germany) and parameters describing shape (circularity, as evaluated by Cowling *et al.*[16]) and size were measured for each t-tubule using ImageJ software. Values were exported into Microsoft Excel (Excel for Mac 2011 version 14.3.9) and Prism software (Prism 6.0, GraphPad Software Inc., La Jolla, CA) for further analysis and graphical representation. Statistical analysis, by mixed effect modeling, was performed with SPSS software (version 2.0.3, IBM, Portsmouth, UK).

Cell lines and tissue culture

A clonal C2C12 myoblast cell line, stably transfected with pGIPZ shRNA construct (V2KLHS_5923 (GCTCATTACTCACAGTATA), Thermo Fisher Scientific) against exon 4 of Hacd1, was evaluated along with an additional clone expressing a control plasmid (RHS4349)[40]. These were grown and differentiated in media containing 2 µg/ml puromycin to select for stable transgene expression in the pGIPZ transfected cells. Cultures were incubated at 37°C in 5% CO_2. Myoblasts were grown in Dulbecco's Modified Eagle Media (DMEM) (Sigma-Aldrich Company Ltd, Dorset, UK) containing 10%

heat inactivated Foetal Bovine Serum (PAA Laboratories, Linz, Austria), 2 mM L-glutamine (Invitrogen), 100 iu/ml penicillin and 0.1 mg/ml streptomycin (Sigma). Cells were plated into tissue culture flasks (Nunc, Thermo Scientific) or hydrophilic-coated optical-bottomed dishes (ibiTreat-coated µ-dishes, Thistle Scientific, Glasgow, UK) for immunocytochemistry and differentiated at 70-80% confluence in DMEM containing 4% heat-inactivated Horse Serum (PAA) and L-glutamine, penicillin and streptomycin as above. In these conditions, a partial rescue of the phenotype previously reported[40] enabled this line of Hacd1-KD myoblasts to form myotubes.

Quantitative RT-PCR was used to compare expression of the skeletal muscle-specific Hacd1 transcript between the control and HACD1-deficient cells. Cells were plated into flasks and harvested as myoblasts and at 2, 7 and 14 days' differentiation. Relative expression of Hacd1 in comparison with Gapdh was evaluated using a modified ΔCT method with efficiency correction[44]. Primer pairs specifically amplified the skeletal muscle Hacd1 full-length isoform (F: 5'-ATGAAGAGAGCGTGGTGCTT-3' R: 5'-AAGGCGGCGTATATTGTGAG-3') for comparison with a house-keeping gene (Gapdh) (F: 5'-TTGTGATGGGTGTGAACCAC-3' R: 5'-TTCAGCTCTGGGATGACCTT-3' 11) that has constant expression during myoblast differentiation[45]. Significant Hacd1 knockdown (approximately 80%) was demonstrated between the Hacd1-KD and shRNA plasmid control cell lines at all time points.

Immunocytochemistry and cell microscopy

Cells plated into optical dishes (ibiTreat-coated µ-dishes) were rinsed in PBS and fixed/permeabilized in methanol:acetone (50:50) for 4 minutes at -20°C (those to be stored prior to staining were allowed to air dry and then kept at -20°C). Immunostaining was performed using primary and secondary antibodies as described for muscle cryosections except nuclei that were labeled with (Hoechst 33342 (Invitrogen) 1:5000 for 5 minutes at room temperature) before mounting with Hydromount (Agar Scientific) using a 19 mm diameter coverslip (VWR, Lutterworth, UK).

Myotube morphology was evaluated (blinded to type) by manual counting performed from two independent experiments per cell line, which generated eight random 10x field of view images from standard areas of RyR1-stained cells at 12 days' differentiation. Significance was evaluated by Fisher's exact test (GraphPad Software Inc.).

Results

Histopathological features of the dogs used in this study and representative of the disease are depicted in figure 1 and table 1. On H&E-stained cryosections, abnormal features of central nucleation, variability in myofiber size, fibrosis and myofiber loss and replacement by fat infiltration were seen in affected HACD1-CNM dogs. Variability in myofiber size with large numbers of small hypotrophic fibers were prominent from the earlier time point (figure 1D) whereas other features, including the proportion of internalized nuclei, became more apparent with increasing age (figure 1G, 1J, 1M and table 1). In normal dogs, oxidative stains have a regular distribution on transverse section within a myofiber and intensity varies based on fiber-type between myofibers (type 1 darker staining) (figure 1B). Abnormal oxidative staining patterns observed in affected dogs included the absence of a clear fiber type distribution and the presence of necklace fibers with an internal, dense-staining ring, running parallel to the sarcolemma, lobulated fibers with dense subsarcolemmal mitochondrial deposits and many fibers with a halo or peripheral rim devoid of oxidative staining (figure 1E, 1H, 1K, 1N). Blinded, subjective scoring revealed that the majority of fibers from HACD1-CNM dogs of all ages had abnormal internal cytoarchitecture with histological and oxidative stains (table 1). The presence of a peripheral halo was a particularly prominent feature in 11 month old dogs (present in around 50% of all fibres) (figure 1N); in older 30 month old dogs this pattern was superseded by more generalized disorganization. Presumed secondary degenerative changes (fat infiltration and fibrosis) were more common in older, compared with younger, dogs (figure 1G, 1J, table 1). Ultrastructural abnormalities observed in affected dogs with HACD1-CNM included internalized or centralized nuclei (figure 1F, 1I, 1L), mitochondrial mislocalization and clumping (figure 1F), presence of lipid bodies (figure 1I, 1L) and myofibrillar disorganization (figure 1I, 1L). These features appeared most severe in the older animals. No significant abnormalities were detected in the heterozygous or control dogs. Prominent features observed by electron microscopy were probed further by immunohistochemistry on cryosections from the same biopsy samples (see below).

Progressive triad abnormalities in HACD1-deficient canine CNM

Recent studies have implicated defective excitation-contraction coupling in the pathogenesis of CNMs linked to mutations in genes other than *HACD1*, and have documented t-tubule abnormalities as a consistent feature in human patients and animal models[11-14,16,18-21]. Consequently, in order to support a link between canine HACD1-CNM and other CNM forms we evaluated the effect of the *HACD1* mutation on muscle membranes in more detail.

Initial subjective evaluation of muscle ultrastructure revealed a proportion of t-tubules that appeared abnormally rounded and dilated in affected dogs (figure 2B-D). Objective morphometric evaluation of shape and size revealed that normal t-tubules were elliptical (circularity [mean of medians ± s.d.] = 0.499 arbitrary units (AU) ± 0.033) with uniform cross-sectional area (0.0021 μm^2 ± 0.0003). In HACD1-CNM 11 month old dogs, circularity and variability was increased (0.755 AU ± 0.045; $p < 0.001$) with an insignificant increase in area (0.0026 μm^2 ± 0.0005; $p = 0.086$). At 30 months of age, both circularity (0.739 AU ± 0.051; $p < 0.001$) and cross sectional area (0.0051 μm^2 ± 0.0008; $p<0.001$) were significantly increased (figure 2E, 2F and supplemental figure 1). In 30 month old dogs, additional membranous abnormalities were observed, including dilated t-tubules with luminal contents (figure 2C, inset).

Disorganization of t-tubule and sarcoplasmic reticulum membrane markers including BIN1 and RyR1

In order to evaluate the distribution of triads in muscle from affected dogs, immunostaining for t-tubule (DHPR) and sarcoplasmic reticulum (SERCA and RyR1) markers was performed on transverse cryosections from the same biopsy samples used for EM. RyR1 and DHPR were observed broadly to colocalize and triad staining was disorganized in HACD1-CNM dogs at both ages. In control dogs, a normal, regular, "honey comb" pattern could be seen outlining the bundles of myofilaments (figure 3A). In affected dogs, the staining was disorganized and density was reduced at the periphery, except for radial remnants directed towards the sarcolemma (figure 3B, 3C). At 30 months old, focal areas of RyR1 and DHPR expression were associated with the periphery of internalized nuclei or were distributed within the sarcoplasm, parallel to the sarcolemma (figure 3C; supplemental figure 2).

Amphiphysin 2 (BIN1), a t-tubule associated protein with a critical role in membrane tubulation and t-tubule development[46], and recruitment of partner proteins[47-49], has disorganized localization in several human CNMs, irrespective of genotype[18]. Double labeling, with antibodies directed against BIN1 and RyR1 (figure 3D-F, supplemental figure 3) revealed a similar pattern of disorganization as seen with DHPR and RyR1 triad staining. Generally, BIN1 and RyR1 colocalized except at the nuclear periphery; some aggregates were positive for BIN1 but not RyR1. In longitudinal sections, areas of intense BIN1- and DHPR-labeling extended from the centralized nucleus (figure 3G-J). Upon reevaluation of the muscle ultrastructure in light of these findings, the prominent subsarcolemmal tubular and vesicular membranous structures tended towards a similar radial alignment and were considered likely to originate from t-tubule and SR networks (figure 3K, 3L).

Thus, dogs with HACD1-CNM display alterations in t-tubule ultrastructure including altered shape and progressive dilation. Triad distribution is increasingly disorganized, with mislocalization especially from areas close to the sarcolemma.

Mitochondrial mislocalization and alterations in membrane trafficking and repair-associated proteins in affected dogs

Mitochondrial mislocalisation and degeneration (as revealed by clumping and whorls) were associated with areas of suspected tubuloreticular membranous abnormalities (figure 3K, 3L). In addition, the peripheral disruption noted on triad staining appeared analogous to that of the halo pattern detected with oxidative histochemistry and this correlation was confirmed using serial sections (figure 4). SERCA2 (figure 4G-I, supplemental figure 4) was used as an additional SR marker that specifically labels the calcium-ATPase in type 1 myofibers. This otherwise colocalized with RyR1 and despite the few remaining type 2 fibers, both fiber types displayed the same pattern of SR disorganization.

Electron microscopy revealed the presence of sarcolemmal abnormalities including membrane invaginations, subsarcolemmal membranous structures including vesicles and caveolae (figure 5A-D). In 11 month old dogs, dysferlin was mislocalized in the cytoplasm in a number of fibers, either diffusely or revealing a peripheral halo (figure 5F,G). Developmental myosin immunolabeling on serial sections revealed that a small proportion of intensely stained fibers with cytoplasmic mislocalization of dysferlin were also positive for this marker of regeneration or immaturity (figure 5H) (commercially available antibodies for embryonic and neonatal myosins do not detect canine isoforms[50]). Adult dogs also displayed cytoplasmic dysferlin expression and an additional pattern, also seen with dystrophin, which suggested the presence of invaginated or internalized sarcolemmal membranes (figure 5K,L). Caveolin 3 had a normal distribution in 11 month old dogs but showed similar abnormalities to dysferlin in adults (30 month old and 14 year old dogs (results not shown)).

Cytoskeletal disorganization

In addition to the membranous defects described above, we also observed more generalized disorganization affecting cytoskeletal and contractile elements. Z-line abnormalities, including accumulations and rods, and myofibrillar disorganization were detected (figure 6A-C) and the

intermediate filament protein, desmin (figure 6G-I), and sarcomeric myosin (figure 6J-L) were mislocalized.

Altered cellular and membrane morphology in HACD1-deficient C2C12 myotubes

We previously showed that myoblast fusion is supported by HACD1 expression[40]. The differentiation conditions used in this study, enabled a partial rescue of the phenotype, allowing us to maintain sarcomeric myosin-positive HACD1-deficient myotubes until 12 days of differentiation (supplemental figure 5). Both control and Hacd1-KD lines formed RyR1-positive myotubes (figure 7B, 7E), but myotubes from the HACD1-deficient line were observed with intracellular vesicles and many had unusual clusters of nuclei that formed complete or partial rings (either in a rounded, multinucleate cell or an area continuous with a more elongated myotube) (figure 7D-F). These clusters of abnormally-positioned myonuclei were associated with an area of intense RyR1 staining (figure 7E). A significantly higher proportion of Hacd1-KD cells exhibited this unusual morphology in comparison with controls (Hacd1-KD 25 out of 147 myotubes versus control 3 out of 229; $P<0.0001$). The skeletal muscle-specific BIN1 isoform (iso-8) had similar localization to that of RyR1: control myotubes were stained relatively homogeneously whereas the Hacd1-KD cells seemed to have focal areas of intense staining, often associated with clusters of nuclei (figure 7F).

Discussion

Canine CNM, a highly prevalent, naturally-occurring, recessive disorder in Labrador Retrievers, is characterized by progressive paresis, absent myotatic reflexes, reduced skeletal muscle mass and histopathological features suggestive of a CNM but the pathophysiology has until now been unclear. In particular, the causative HACD1 mutation's impact on muscle ultrastructure and subcellular membrane systems, which are implicated in CNMs with different genetic causes, has not previously been investigated. Our work reveals a fundamental role for HACD1 in the maintenance of these structures in skeletal muscle. Further we demonstrate that this large animal model displays numerous pathological features that are closely related to those in human CNMs and smaller laboratory animal CNM models. Our work helps explain the progressive paresis displayed by affected dogs and provides mechanistic insight into a rare, but related human congenital myopathy with closely related clinical features[32].

Canine HACD1-deficiency and triad abnormalities link to proposed pathogenesis for other CNMs

In skeletal muscle, numerous highly specialized membrane systems interact to convey neuronal input via the neuromuscular junction, conduct these signals internally via t-tubules, and store and release calcium to activate the contractile apparatus and transmit the generated force to the extracellular matrix. Since 2009, t-tubule abnormalities have been described consistently in human patients or animal models with defects in CNM-associated genes[15]: *MTM1*[11-13]; *BIN1*[17,18,21,51]; *DNM2*[14,16,18]; *hJUMPY*[19,52] and *RYR1*[22,53]. In our work, t-tubules from HACD1-deficient CNM dogs at both ages were more circular in transverse-section at triads when compared with controls and became significantly larger by 30 months of age. The initial alteration in shape and subsequent dilation suggest that t-tubules remodel or undergo degradative morphological changes in dogs affected by HACD1-CNM. Our identification of apparent membranous contents within the lumen of some t-tubules has not been reported in other myopathies to our knowledge. Immunohistochemistry revealed triad-associated proteins, DHPR and RyR1, were disorganized and depleted from the myofiber periphery. Our results reveal that, as for other CNM-associated genes including *MTM1*, *DNM2* and *BIN1*[11,12,14,21,54], HACD1 has a functional role in the maintenance of t-tubule morphology and localization, either directly or indirectly.

This current study extensively characterized t-tubule morphology in HACD1-CNM; dilated junctional SR terminals were also documented with prominent membranous structures in the intermyofibrillar space and within myofibrillar bundles that might represent aberrant SR membranes (figure 5C, 5D, 6D and 6E). These abnormalities were probed further by immunohistochemistry to examine the t-system and SR distribution, organization and physical coupling. Markers for junctional and longitudinal SR (RyR1 and SERCA2 respectively[55]) were disorganized, as were proteins localized to t-tubules (DHPR[55] and BIN1[56]). SERCA2 immunostaining also enabled identification of type 1 myofibers and, whilst there is a marked shift towards oxidative fibers in this condition, SR defects were identified in both fiber types. RyR1, DHPR and BIN1 aggregates, similar to those reported here, have been detected previously in canine models of X-linked MTM[13] and BIN1 AR CNM[18,21]. A recent report localized MTM1 to junctional SR and concluded that altered SR remodeling is likely to be a primary cause of intracellular membrane disorganization in myotubular myopathy[20]. BIN1 localises to t-tubules and has a role in their formation[46,47]. HACD1 is believed to reside with other components of the elongase complex at ER/SR membranes[34,40]; however the localization and specific function(s) of VLCFA and related lipids in muscle remain to be fully characterized. It is not surprising - given the intimate association between

tubuloreticular membrane networks - that defects in one will impact the other, producing similar triad abnormalities.

We have also provided evidence for similar membranous abnormalities in Hacd1-KD C2C12 myotubes, which displayed intracellular vacuoles visible by light microscopy and accumulations of RyR1- and BIN1-positive structures in conjunction with abnormally-positioned nuclei. Whilst this intermediate (myotube) developmental stage in C2C12 cells precedes organized tubuloreticular networks, rudimentary structures are present[46,57-59]. These results link HACD1-deficiency in dogs with CNM and a cell culture model, to abnormal development and maintenance of triad membranes and BIN1-mislocalisation. These are consistent features currently considered to be of primary importance in the pathogenesis of CNMs[15,18] and, via postulated dysfunction of excitation-contraction coupling, provide a common mechanism for paresis and hypotonia in this group of conditions and a potential target for therapeutic intervention.

Generalized membranous and cytoskeletal defects are apparent in HACD1-CNM

Sarcolemmal membrane abnormalities were also apparent in CNM-affected dogs: these included dilated tubular and vesicular structures; membrane invaginations and caveolae - very similar findings are also apparent in other CNMs[18]. Dysferlin and caveolin 3 associate with one another at the sarcolemma in mature skeletal muscle: they localize to the developing t-tubule system and are involved in membrane trafficking and repair[60-62]. Dysferlinopathies are associated with morphological abnormalities in t-tubules[61]. Several recent reports have documented abnormal localization of one or both of these proteins in autosomal CNMs[14,21,63]: in particular, the cytoplasmic mislocalization and sarcolemmal invaginations apparent with dysferlin immunostaining in CNM-affected dogs in this study are similar to those reported in the AR CNM associated with a *BIN1* mutation in Great Dane dogs[21]. In the current study, the pattern of cytoplasmic dysferlin staining often displayed a similar halo pattern to that observed in triad and oxidative stains, which might suggest that dysferlin localizes to the t-tubule system in these fibers for membrane trafficking and repair. Olby *et al.*[64] previously evaluated dysferlin in muscle from affected Labradors by western blotting but did not detect any difference in total expression compared with controls.

Mislocalization of desmin, the major intermediate filament protein in skeletal muscle, is well documented in congenital myopathies in general and in CNMs in particular, where accumulations are associated with the centralized nucleus[1,2,65,66]. A direct role in intermediate filament organization and

maintenance, independent of defective phosphatase activity, has been documented for MTM1[67]. Such cytoskeletal disorganization might also affect mitochondrial localization and dynamics[67] perhaps explaining the abnormal mitochondrial distribution in HACD1-CNM dogs. Progressive derangement of the contractile apparatus in HACD1-CNM dogs was indicated by the Z-line abnormalities, including accumulations and rods, and myofibrillar disorganization detected by electron microscopy and by the altered immunofluorescence-staining pattern for sarcomeric myosin. Interestingly, in affected dogs, an area around the nucleus was often devoid of myofilaments regardless of positioning - this was not the case in the controls (figure 6). BIN1 was recently shown to bind both the nuclear envelope protein nesprin and the microtubule associated protein CLIP170 implicating a role for this CNM-associated protein in nuclear positioning[49]. The interaction of the cytoskeleton and nuclear anchoring proteins, mechanisms that control myonuclear positioning and the impact of abnormal nuclear internalization on muscle function are exciting areas for further research in CNM[68,69].

Cytoarchitectural rearrangements have long been recognized as features of CNM and are often most obvious as unusual oxidative staining patterns (such as radial strands or necklaces)[70]. As in canine CNM, centralized nuclei are often surrounded by areas devoid of myofilaments that contain accumulations of mitochondria, glycogen and SR membranes[70]. As intracellular systems do not exist in isolation, disorganization of internal membranes - in particular the SR, which interacts with numerous organelles - would be expected to affect positioning of other compartments[20,55]. Nonetheless, involvement of CNM-associated proteins in other complex protein-protein interactions is being increasingly documented[49,67,69,71]. Extensive myofibrillar disorganization and nuclear internalization were initially described as part of the spectrum of congenital myopathies attributable to *RYR1* mutations[72] and more recently mutations in the *TTN* gene encoding titin have been found to cause similar pathology[10]. A mechanism for their development from areas of altered Ca^{2+} homeostasis has been proposed after following the progression of core development in *Ryr1*-mutant mice[53,73].

Disrupted lipid metabolism and membrane trafficking present a unifying pathophysiological model for CNMs

There is compelling experimental evidence of aberrant membrane trafficking from models of classical (MTM1-, BIN1-, DNM2- and RyR1-associated) CNMs[5,12,15,18,20,74]. We propose that HACD1 deficiency affects VLCFA biosynthesis[32,34,40] leading to altered t-tubule, SR or sarcolemmal membrane properties and ultimately progressive dysfunction and degeneration of these muscle membranes. VLCFA are

components of complex lipids with important structural and signaling roles[75]. VLCFA-substituted phosphatidylinositol is thought to be important in stabilizing highly curved membranes as the very long FA chains might associate with both sides of the lipid bilayer and fill areas left void where carbon chains are unopposed due to extreme curvature[76]. Blondelle *et al.*,[40] recently documented alterations in VLCFA:LCFA and unsaturated:saturated fatty acid ratios in HACD1-deficient models which reduced plasma membrane fluidity resulting in defective membrane fusion and impaired early myogenesis. A similar mechanism could account for the abnormalities and progressive degeneration in t-tubule membranes as fusion is required for t-tubule development (elongation), repair and maintenance[15]. Defects in *Phs1* (the yeast homologue of *HACD1*) lead to abnormalities in a number of signaling molecules – in particular, reduced concentrations of complex sphingolipids and PI monophosphates - which notably include PI3P, the major substrate of myotubularin[34]. Membrane defects are emerging as consistent features in CNM[3,18,74], therefore these findings lend additional credence to the inclusion of canine CNM in this classification and validate it as a potential large animal model for translational research.

Lin *et al.*[35] and Blondelle *et al.*[40] both documented severely impaired differentiation in HACD1-deficient myoblasts, but, in contrast, here we reveal progressive age-associated muscle degeneration in CNM-affected dogs. Similarly, other CNM-associated proteins (MTM1 and BIN1) have been shown to have roles in both development[12,46,77,78] and in maintenance[11,13,17,66,79,80] of the complex membrane systems in mature muscle. In HACD1-deficient dogs, early differentiation of muscle might be partially rescued by expression from various paralogous genes, in particular, other HACD enzymes (such as ubiquitously-expressed HACD2/PTPLB or HACD3/PTPLAD1)[34], and perhaps maternal delivery of VLCFA via the placenta and milk[81]. We hypothesize that culture conditions employed in this study overcame a defect in cell fusion, allowing us to detect (at a later stage of differentiation), defective internal membrane system formation or maintenance.

Mutation of HACD1 in humans has been reported in a single consanguineous family and resulted in a congenital myopathy with fiber type disproportion[32]. Patients exhibited neonatal hypotonia and a severely myopathic phenotype that gradually improved – the single case evaluated in adulthood had normal gait however the absence of myotatic reflexes persisted. This is distinct to the progressive clinical course observed during growth in dogs with HACD1 deficiency which is perhaps attributed to different effects of the two mutations on expression and function of HACD1: canine CNM is caused by an insertion that affects splicing and reduces expression of normal isoforms to <1% of normal[29]

whereas in the human family there was a C-terminal nonsense mutation that reduced expression to 30% of normal levels and produced an abnormally glycosylated protein[32]. Alternatively, species-related phenotypic variation may relate to differences in dietary fatty acid composition and lipid metabolism or muscle development (the latter has been suggested for *MTM1* mutations in humans, mice and dogs to explain a similar discrepancy in age of onset and progression[13]). Pathological features associated with the human *HACD1* mutation, in common with canine CNM, included the presence of hypotrophic fibers and a marked a predominance of type 1 myofibers[32]. An increased proportion of centralized nuclei was not identified but pathological description was limited to two patients with muscle biopsy samples taken at a young age (1-2 years). The proportion of centralized nuclei in affected dogs is often not dramatically elevated at the time of diagnosis[31] and increases progressively over time; the same might be true in affected human patients as they age. Dogs, mice[40] and humans[32] with loss-of-function mutations in HACD1 display congenital myopathy with several shared clinical and pathological features: *HACD1* should therefore be considered a candidate gene for congenital fiber type disproportion syndromes, and congenital and CNMs in humans and other species.

In conclusion, dogs with HACD1 deficiency have ultrastructural abnormalities in membranes, in particular in t-tubules and SR - a hallmark of classical CNM that is thought to be key factor in human disease symptomatology and pathogenesis. In addition, they also replicate a number of other prominent pathological features of this group of disorders. Our confirmation of this additional gene/protein as a cause of CNM enhances our understanding of the pathogenesis of these disorders. Furthermore, cementing the link between HACD1-deficiency and CNM provides mechanistic insight into the role of HACD/VLCFA in membrane trafficking and tubuloreticular membrane maintenance in muscle - which is of fundamental and pressing importance now that this gene has been linked to a congenital myopathy in humans[32]. Finally, our work helps explain the profound and progressive paresis observed in the most prevalent inherited myopathy of Labrador Retrievers, the most popular dog breed worldwide.

Acknowledgements

We are grateful to Dr Ruby Chang (RVC) for statistical support. The authors thank Dr Susan Brown (RVC) and Ms Claire Massey (RVC) for advice with histological and histochemical staining and electron microscopy. We also thank Mr Laurent Guillaud for technical assistance and Dr Pablo Aguilar, Mr Xavier Cauchois and the team who care for the dogs at the Laboratoire de Neurobiologie of EnvA. This manuscript

was approved by the Royal Veterinary College's research office and allocated manuscript number CSS_01143.

References

[1] Dubowitz V, Sewry C: Muscle Biopsy: A Practical Approach. 3rd Edition ed. Philadelphia, USA: Elsevier, Saunders, 2007.

[2] Romero N, Laporte J: Centronucelar myopathies. Muscle disease : pathology and genetics. Edited by Goebel HH, Sewry CA, Weller RO. Second edition. ed. Chichester: Wiley-Blackwell, 2013. pp. 134-44.

[3] Jungbluth H, Gautel M: Pathogenic mechanisms in centronuclear myopathies. Frontiers in aging neuroscience 2014, 6:339.

[4] Laporte J, Hu LJ, Kretz C, Mandel JL, Kioschis P, Coy JF, Klauck SM, Poustka A, Dahl N: A gene mutated in X-linked myotubular myopathy defines a new putative tyrosine phosphatase family conserved in yeast. Nat Genet 1996, 13:175-82.

[5] Nicot AS, Toussaint A, Tosch V, Kretz C, Wallgren-Pettersson C, Iwarsson E, Kingston H, Garnier JM, Biancalana V, Oldfors A, Mandel JL, Laporte J: Mutations in amphiphysin 2 (BIN1) disrupt interaction with dynamin 2 and cause autosomal recessive centronuclear myopathy. Nat Genet 2007, 39:1134-9.

[6] Bitoun M, Maugenre S, Jeannet PY, Lacene E, Ferrer X, Laforet P, Martin JJ, Laporte J, Lochmuller H, Beggs AH, Fardeau M, Eymard B, Romero NB, Guicheney P: Mutations in dynamin 2 cause dominant centronuclear myopathy. Nat Genet 2005, 37:1207-9.

[7] Jungbluth H, Zhou H, Sewry CA, Robb S, Treves S, Bitoun M, Guicheney P, Buj-Bello A, Bonnemann C, Muntoni F: Centronuclear myopathy due to a de novo dominant mutation in the skeletal muscle ryanodine receptor (RYR1) gene. Neuromuscul Disord 2007, 17:338-45.

[8] Majczenko K, Davidson AE, Camelo-Piragua S, Agrawal PB, Manfready RA, Li X, Joshi S, Xu J, Peng W, Beggs AH, Li JZ, Burmeister M, Dowling JJ: Dominant mutation of CCDC78 in a unique congenital myopathy with prominent internal nuclei and atypical cores. Am J Hum Genet 2012, 91:365-71.

[9] Agrawal PB, Pierson CR, Joshi M, Liu X, Ravenscroft G, Moghadaszadeh B, Talabere T, Viola M, Swanson LC, Haliloglu G, Talim B, Yau KS, Allcock RJ, Laing NG, Perrella MA, Beggs AH: SPEG interacts with myotubularin, and its deficiency causes centronuclear myopathy with dilated cardiomyopathy. Am J Hum Genet 2014, 95:218-26.

[10] Ceyhan-Birsoy O, Agrawal PB, Hidalgo C, Schmitz-Abe K, DeChene ET, Swanson LC, Soemedi R, Vasli N, Iannaccone ST, Shieh PB, Shur N, Dennison JM, Lawlor MW, Laporte J, Markianos K, Fairbrother

572 WG, Granzier H, Beggs AH: Recessive truncating titin gene, TTN, mutations presenting as centronuclear
573 myopathy. Neurology 2013, 81:1205-14.
574 [11] Al-Qusairi L, Weiss N, Toussaint A, Berbey C, Messaddeq N, Kretz C, Sanoudou D, Beggs AH, Allard
575 B, Mandel JL, Laporte J, Jacquemond V, Buj-Bello A: T-tubule disorganization and defective excitation-
576 contraction coupling in muscle fibers lacking myotubularin lipid phosphatase. Proc Natl Acad Sci U S A
577 2009, 106:18763-8.
578 [12] Dowling JJ, Vreede AP, Low SE, Gibbs EM, Kuwada JY, Bonnemann CG, Feldman EL: Loss of
579 myotubularin function results in T-tubule disorganization in zebrafish and human myotubular myopathy.
580 PLoS Genet 2009, 5:e1000372.
581 [13] Beggs AH, Bohm J, Snead E, Kozlowski M, Maurer M, Minor K, Childers MK, Taylor SM, Hitte C,
582 Mickelson JR, Guo LT, Mizisin AP, Buj-Bello A, Tiret L, Laporte J, Shelton GD: MTM1 mutation associated
583 with X-linked myotubular myopathy in Labrador Retrievers. Proc Natl Acad Sci U S A 2010, 107:14697-
584 702.
585 [14] Durieux AC, Vignaud A, Prudhon B, Viou MT, Beuvin M, Vassilopoulos S, Fraysse B, Ferry A, Laine
586 J, Romero NB, Guicheney P, Bitoun M: A centronuclear myopathy-dynamin 2 mutation impairs skeletal
587 muscle structure and function in mice. Hum Mol Genet 2010, 19:4820-36.
588 [15] Al-Qusairi L, Laporte J: T-tubule biogenesis and triad formation in skeletal muscle and implication in
589 human diseases. Skelet Muscle 2011, 1:26.
590 [16] Cowling BS, Toussaint A, Amoasii L, Koebel P, Ferry A, Davignon L, Nishino I, Mandel JL, Laporte J:
591 Increased expression of wild-type or a centronuclear myopathy mutant of dynamin 2 in skeletal muscle of
592 adult mice leads to structural defects and muscle weakness. Am J Pathol 2011, 178:2224-35.
593 [17] Tjondrokoesoemo A, Park KH, Ferrante C, Komazaki S, Lesniak S, Brotto M, Ko JK, Zhou J,
594 Weisleder N, Ma J: Disrupted membrane structure and intracellular Ca(2)(+) signaling in adult skeletal
595 muscle with acute knockdown of Bin1. PLoS One 2011, 6:e25740.
596 [18] Toussaint A, Cowling BS, Hnia K, Mohr M, Oldfors A, Schwab Y, Yis U, Maisonobe T, Stojkovic T,
597 Wallgren-Pettersson C, Laugel V, Echaniz-Laguna A, Mandel JL, Nishino I, Laporte J: Defects in
598 amphiphysin 2 (BIN1) and triads in several forms of centronuclear myopathies. Acta Neuropathol 2011,
599 121:253-66.
600 [19] Hnia K, Kretz C, Amoasii L, Bohm J, Liu X, Messaddeq N, Qu CK, Laporte J: Primary T-tubule and
601 autophagy defects in the phosphoinositide phosphatase Jumpy/MTMR14 knockout mice muscle. Adv Biol
602 Regul 2012, 52:98-107.

603 [20] Amoasii L, Hnia K, Chicanne G, Brech A, Cowling BS, Muller MM, Schwab Y, Koebel P, Ferry A,
604 Payrastre B, Laporte J: Myotubularin and PtdIns3P remodel the sarcoplasmic reticulum in muscle in vivo.
605 J Cell Sci 2013, 126:1806-19.
606 [21] Bohm J, Vasli N, Maurer M, Cowling B, Shelton GD, Kress W, Toussaint A, Prokic I, Schara U,
607 Anderson TJ, Weis J, Tiret L, Laporte J: Altered splicing of the BIN1 muscle-specific exon in humans and
608 dogs with highly progressive centronuclear myopathy. PLoS Genet 2013, 9:e1003430.
609 [22] Zhou H, Rokach O, Feng L, Munteanu I, Mamchaoui K, Wilmshurst JM, Sewry C, Manzur AY, Pillay
610 K, Mouly V, Duchen M, Jungbluth H, Treves S, Muntoni F: RyR1 deficiency in congenital myopathies
611 disrupts excitation-contraction coupling. Hum Mutat 2013, 34:986-96.
612 [23] Durieux AC, Vassilopoulos S, Laine J, Fraysse B, Brinas L, Prudhon B, Castells J, Freyssenet D,
613 Bonne G, Guicheney P, Bitoun M: A centronuclear myopathy--dynamin 2 mutation impairs autophagy in
614 mice. Traffic 2012, 13:869-79.
615 [24] Kramer JW, Hegreberg GA, Bryan GM, Meyers K, Ott RL: A muscle disorder of Labrador retrievers
616 characterized by deficiency of type II muscle fibers. J Am Vet Med Assoc 1976, 169:817-20.
617 [25] Shelton GD: What's new in muscle and peripheral nerve diseases? Vet Comp Orthop Traumatol
618 2007, 20:249-55.
619 [26] Maurer M, Mary J, Guillaud L, Fender M, Pele M, Bilzer T, Olby N, Penderis J, Shelton GD, Panthier
620 JJ, Thibaud JL, Barthelemy I, Aubin-Houzelstein G, Blot S, Hitte C, Tiret L: Centronuclear myopathy in
621 Labrador retrievers: a recent founder mutation in the PTPLA gene has rapidly disseminated worldwide.
622 PLoS One 2012, 7:e46408.
623 [27] Blot S, Tiret L, Devillaire A, Fardeau M, Dreyfus PA: Phenotypic Description of a Canine
624 Centronuclear Myopathy. Journal of the Neurological Sciences 2002, 199:S9.
625 [28] Tiret L, Blot S, Kessler JL, Gaillot H, Breen M, Panthier JJ: The cnm locus, a canine homologue of
626 human autosomal forms of centronuclear myopathy, maps to chromosome 2. Hum Genet 2003, 113:297-
627 306.
628 [29] Pele M, Tiret L, Kessler JL, Blot S, Panthier JJ: SINE exonic insertion in the PTPLA gene leads to
629 multiple splicing defects and segregates with the autosomal recessive centronuclear myopathy in dogs.
630 Hum Mol Genet 2005, 14:1417-27.
631 [30] McKerrell R, Braund KG: Hereditary myopathy in Labrador Retrievers: clinical variations. Journal of
632 Small Animal Practice 1987, 28:479-89.
633 [31] McKerrell RE, Braund KG: Hereditary myopathy in Labrador retrievers: a morphologic study. Vet
634 Pathol 1986, 23:411-7.

635 [32] Muhammad E, Reish O, Ohno Y, Scheetz T, Deluca A, Searby C, Regev M, Benyamini L, Fellig Y,
636 Kihara A, Sheffield VC, Parvari R: Congenital myopathy is caused by mutation of HACD1. Hum Mol Genet
637 2013.
638 [33] Uwanogho DA, Hardcastle Z, Balogh P, Mirza G, Thornburg KL, Ragoussis J, Sharpe PT: Molecular
639 cloning, chromosomal mapping, and developmental expression of a novel protein tyrosine phosphatase-
640 like gene. Genomics 1999, 62:406-16.
641 [34] Ikeda M, Kanao Y, Yamanaka M, Sakuraba H, Mizutani Y, Igarashi Y, Kihara A: Characterization of
642 four mammalian 3-hydroxyacyl-CoA dehydratases involved in very long-chain fatty acid synthesis. FEBS
643 Lett 2008, 582:2435-40.
644 [35] Lin X, Yang X, Li Q, Ma Y, Cui S, He D, Schwartz RJ, Chang J: Protein tyrosine phosphatase-like A
645 regulates myoblast proliferation and differentiation through MyoG and the cell cycling signaling pathway.
646 Mol Cell Biol 2012, 32:297-308.
647 [36] Denic V, Weissman JS: A molecular caliper mechanism for determining very long-chain fatty acid
648 length. Cell 2007, 130:663-77.
649 [37] Kihara A, Sakuraba H, Ikeda M, Denpoh A, Igarashi Y: Membrane topology and essential amino acid
650 residues of Phs1, a 3-hydroxyacyl-CoA dehydratase involved in very long-chain fatty acid elongation. J
651 Biol Chem 2008, 283:11199-209.
652 [38] Sabbadini RA, Danieli-Betto D, Betto R: The role of sphingolipids in the control of skeletal muscle
653 function: a review. Italian journal of neurological sciences 1999, 20:423-30.
654 [39] Balla T: Phosphoinositides: tiny lipids with giant impact on cell regulation. Physiol Rev 2013, 93:1019-
655 137.
656 [40] Blondelle J, Ohno Y, Gache V, Guyot S, Storck S, Blanchard-Gutton N, Barthelemy I, Walmsley G,
657 Rahier A, Gadin S, Maurer M, Guillaud L, Prola A, Ferry A, Aubin-Houzelstein G, Demarquoy J, Relaix F,
658 Piercy RJ, Blot S, Kihara A, Tiret L, Pilot-Storck F: HACD1, a regulator of membrane composition and
659 fluidity, promotes myoblast fusion and skeletal muscle growth. Journal of molecular cell biology 2015,
660 7:429-40.
661 [41] Bach L, Michaelson LV, Haslam R, Bellec Y, Gissot L, Marion J, Da Costa M, Boutin JP, Miquel M,
662 Tellier F, Domergue F, Markham JE, Beaudoin F, Napier JA, Faure JD: The very-long-chain hydroxy fatty
663 acyl-CoA dehydratase PASTICCINO2 is essential and limiting for plant development. Proc Natl Acad Sci U
664 S A 2008, 105:14727-31.
665 [42] Molino D, Van der Giessen E, Gissot L, Hematy K, Marion J, Barthelemy J, Bellec Y, Vernhettes S,
666 Satiat-Jeunemaitre B, Galli T, Tareste D, Faure JD: Inhibition of very long acyl chain sphingolipid

667 synthesis modifies membrane dynamics during plant cytokinesis. Biochim Biophys Acta 2014, 1842:1422-
668 30.
669 [43] Walmsley GL, Arechavala-Gomeza V, Fernandez-Fuente M, Burke MM, Nagel N, Holder A, Stanley
670 R, Chandler K, Marks SL, Muntoni F, Shelton GD, Piercy RJ: A duchenne muscular dystrophy gene hot
671 spot mutation in dystrophin-deficient cavalier king charles spaniels is amenable to exon 51 skipping. PLoS
672 One 2010, 5:e8647.
673 [44] Pfaffl MW, Horgan GW, Dempfle L: Relative expression software tool (REST) for group-wise
674 comparison and statistical analysis of relative expression results in real-time PCR. Nucleic Acids Res
675 2002, 30:e36.
676 [45] Nishimura M, Nikawa T, Kawano Y, Nakayama M, Ikeda M: Effects of dimethyl sulfoxide and
677 dexamethasone on mRNA expression of housekeeping genes in cultures of C2C12 myotubes. Biochem
678 Biophys Res Commun 2008, 367:603-8.
679 [46] Lee E, Marcucci M, Daniell L, Pypaert M, Weisz OA, Ochoa GC, Farsad K, Wenk MR, De Camilli P:
680 Amphiphysin 2 (Bin1) and T-tubule biogenesis in muscle. Science 2002, 297:1193-6.
681 [47] Royer B, Hnia K, Gavriilidis C, Tronchere H, Tosch V, Laporte J: The myotubularin-amphiphysin 2
682 complex in membrane tubulation and centronuclear myopathies. EMBO Rep 2013.
683 [48] Picas L, Viaud J, Schauer K, Vanni S, Hnia K, Fraisier V, Roux A, Bassereau P, Gaits-Iacovoni F,
684 Payrastre B, Laporte J, Manneville JB, Goud B: BIN1/M-Amphiphysin2 induces clustering of
685 phosphoinositides to recruit its downstream partner dynamin. Nature communications 2014, 5:5647.
686 [49] D'Alessandro M, Hnia K, Gache V, Koch C, Gavriilidis C, Rodriguez D, Nicot AS, Romero NB,
687 Schwab Y, Gomes E, Labouesse M, Laporte J: Amphiphysin 2 Orchestrates Nucleus Positioning and
688 Shape by Linking the Nuclear Envelope to the Actin and Microtubule Cytoskeleton. Dev Cell 2015, 35:186-
689 98.
690 [50] Strbenc M, Smerdu V, Pogacnik A, Fazarinc G: Myosin heavy chain isoform transitions in canine
691 skeletal muscles during postnatal growth. J Anat 2006, 209:149-63.
692 [51] Fugier C, Klein AF, Hammer C, Vassilopoulos S, Ivarsson Y, Toussaint A, Tosch V, Vignaud A, Ferry
693 A, Messaddeq N, Kokunai Y, Tsuburaya R, de la Grange P, Dembele D, Francois V, Precigout G,
694 Boulade-Ladame C, Hummel MC, Lopez de Munain A, Sergeant N, Laquerriere A, Thibault C, Deryckere
695 F, Auboeuf D, Garcia L, Zimmermann P, Udd B, Schoser B, Takahashi MP, Nishino I, Bassez G, Laporte
696 J, Furling D, Charlet-Berguerand N: Misregulated alternative splicing of BIN1 is associated with T tubule
697 alterations and muscle weakness in myotonic dystrophy. Nat Med 2011, 17:720-5.

698 [52] Dowling JJ, Low SE, Busta AS, Feldman EL: Zebrafish MTMR14 is required for excitation-contraction
699 coupling, developmental motor function and the regulation of autophagy. Hum Mol Genet 2010, 19:2668-
700 81.
701 [53] Boncompagni S, Rossi AE, Micaroni M, Hamilton SL, Dirksen RT, Franzini-Armstrong C, Protasi F:
702 Characterization and temporal development of cores in a mouse model of malignant hyperthermia. Proc
703 Natl Acad Sci U S A 2009, 106:21996-2001.
704 [54] Razzaq A, Robinson IM, McMahon HT, Skepper JN, Su Y, Zelhof AC, Jackson AP, Gay NJ, O'Kane
705 CJ: Amphiphysin is necessary for organization of the excitation-contraction coupling machinery of
706 muscles, but not for synaptic vesicle endocytosis in Drosophila. Genes Dev 2001, 15:2967-79.
707 [55] Franzini-Armstrong C, Engel A: Skeletal Muscle: Architecture of Membrane Systems. Muscle:
708 Fundamental Biology and Mechanisms of Disease. Edited by Hill J, Olson E. London, UK: Elsevier
709 Academic Press, 2012. pp. 763-74.
710 [56] Butler MH, David C, Ochoa GC, Freyberg Z, Daniell L, Grabs D, Cremona O, De Camilli P:
711 Amphiphysin II (SH3P9; BIN1), a member of the amphiphysin/Rvs family, is concentrated in the cortical
712 cytomatrix of axon initial segments and nodes of ranvier in brain and around T tubules in skeletal muscle.
713 J Cell Biol 1997, 137:1355-67.
714 [57] Parton RG, Way M, Zorzi N, Stang E: Caveolin-3 associates with developing T-tubules during muscle
715 differentiation. J Cell Biol 1997, 136:137-54.
716 [58] Carozzi AJ, Ikonen E, Lindsay MR, Parton RG: Role of cholesterol in developing T-tubules: analogous
717 mechanisms for T-tubule and caveolae biogenesis. Traffic 2000, 1:326-41.
718 [59] Nori A, Valle G, Bortoloso E, Turcato F, Volpe P: Calsequestrin targeting to sarcoplasmic reticulum of
719 skeletal muscle fibers. Am J Physiol Cell Physiol 2006, 291:C245-53.
720 [60] Bansal D, Miyake K, Vogel SS, Groh S, Chen CC, Williamson R, McNeil PL, Campbell KP: Defective
721 membrane repair in dysferlin-deficient muscular dystrophy. Nature 2003, 423:168-72.
722 [61] Klinge L, Harris J, Sewry C, Charlton R, Anderson L, Laval S, Chiu YH, Hornsey M, Straub V, Barresi
723 R, Lochmuller H, Bushby K: Dysferlin associates with the developing T-tubule system in rodent and
724 human skeletal muscle. Muscle Nerve 2010, 41:166-73.
725 [62] Sinha B, Koster D, Ruez R, Gonnord P, Bastiani M, Abankwa D, Stan RV, Butler-Browne G, Vedie B,
726 Johannes L, Morone N, Parton RG, Raposo G, Sens P, Lamaze C, Nassoy P: Cells respond to
727 mechanical stress by rapid disassembly of caveolae. Cell 2011, 144:402-13.
728 [63] Bohm J, Biancalana V, Malfatti E, Dondaine N, Koch C, Vasli N, Kress W, Strittmatter M, Taratuto AL,
729 Gonorazky H, Laforet P, Maisonobe T, Olive M, Gonzalez-Mera L, Fardeau M, Carriere N, Clavelou P,

730 Eymard B, Bitoun M, Rendu J, Faure J, Weis J, Mandel JL, Romero NB, Laporte J: Adult-onset autosomal
731 dominant centronuclear myopathy due to BIN1 mutations. Brain 2014, 137:3160-70.
732 [64] Olby NJ, Sharp NJ, Anderson LV, Kunkel LM, Bonnemann CG: Evaluation of the dystrophin-
733 glycoprotein complex, alpha-actinin, dysferlin and calpain 3 in an autosomal recessive muscular dystrophy
734 in Labrador retrievers. Neuromuscul Disord 2001, 11:41-9.
735 [65] Manta P, Mamali I, Zambelis T, Aquaviva T, Kararizou E, Kalfakis N: Immunocytochemical study of
736 cytoskeletal proteins in centronuclear myopathies. Acta Histochem 2006, 108:271-6.
737 [66] Joubert R, Vignaud A, Le M, Moal C, Messaddeq N, Buj-Bello A: Site-specific Mtm1 mutagenesis by
738 an AAV-Cre vector reveals that myotubularin is essential in adult muscle. Hum Mol Genet 2013, 22:1856-
739 66.
740 [67] Hnia K, Tronchere H, Tomczak KK, Amoasii L, Schultz P, Beggs AH, Payrastre B, Mandel JL, Laporte
741 J: Myotubularin controls desmin intermediate filament architecture and mitochondrial dynamics in human
742 and mouse skeletal muscle. J Clin Invest 2011, 121:70-85.
743 [68] Metzger T, Gache V, Xu M, Cadot B, Folker ES, Richardson BE, Gomes ER, Baylies MK: MAP and
744 kinesin-dependent nuclear positioning is required for skeletal muscle function. Nature 2012, 484:120-4.
745 [69] Falcone S, Roman W, Hnia K, Gache V, Didier N, Laine J, Aurade F, Marty I, Nishino I, Charlet-
746 Berguerand N, Romero NB, Marazzi G, Sassoon D, Laporte J, Gomes ER: N-WASP is required for
747 Amphiphysin-2/BIN1-dependent nuclear positioning and triad organization in skeletal muscle and is
748 involved in the pathophysiology of centronuclear myopathy. EMBO molecular medicine 2014, 6:1455-75.
749 [70] Romero NB: Centronuclear myopathies: a widening concept. Neuromuscul Disord 2010, 20:223-8.
750 [71] Ferguson SM, De Camilli P: Dynamin, a membrane-remodelling GTPase. Nat Rev Mol Cell Biol 2012,
751 13:75-88.
752 [72] Bevilacqua JA, Monnier N, Bitoun M, Eymard B, Ferreiro A, Monges S, Lubieniecki F, Taratuto AL,
753 Laquerriere A, Claeys KG, Marty I, Fardeau M, Guicheney P, Lunardi J, Romero NB: Recessive RYR1
754 mutations cause unusual congenital myopathy with prominent nuclear internalization and large areas of
755 myofibrillar disorganization. Neuropathol Appl Neurobiol 2011, 37:271-84.
756 [73] Jungbluth H, Dowling JJ, Ferreiro A, Muntoni F: 182nd ENMC International Workshop: RYR1-related
757 myopathies, 15-17th April 2011, Naarden, The Netherlands. Neuromuscul Disord 2012, 22:453-62.
758 [74] Cowling BS, Toussaint A, Muller J, Laporte J: Defective membrane remodeling in neuromuscular
759 diseases: insights from animal models. PLoS Genet 2012, 8:e1002595.
760 [75] Kihara A: Very long-chain fatty acids: elongation, physiology and related disorders. J Biochem 2012,
761 152:387-95.

[76] Schneiter R, Brugger B, Amann CM, Prestwich GD, Epand RF, Zellnig G, Wieland FT, Epand RM: Identification and biophysical characterization of a very-long-chain-fatty-acid-substituted phosphatidylinositol in yeast subcellular membranes. Biochem J 2004, 381:941-9.

[77] Lawlor MW, Alexander MS, Viola MG, Meng H, Joubert R, Gupta V, Motohashi N, Manfready RA, Hsu CP, Huang P, Buj-Bello A, Kunkel LM, Beggs AH, Gussoni E: Myotubularin-deficient myoblasts display increased apoptosis, delayed proliferation, and poor cell engraftment. Am J Pathol 2012, 181:961-8.

[78] Shichiji M, Biancalana V, Fardeau M, Hogrel J, Osawa M, Laporte J, Romero N: Extensive morphological and immunohistochemical characterization in myotubular myopathy. Brain and Behaviour 2013, 3:476-86.

[79] Buj-Bello A, Laugel V, Messaddeq N, Zahreddine H, Laporte J, Pellissier JF, Mandel JL: The lipid phosphatase myotubularin is essential for skeletal muscle maintenance but not for myogenesis in mice. Proc Natl Acad Sci U S A 2002, 99:15060-5.

[80] Hamanaka K, Inami I, Wada T, Mitsuhshi S, Noguchi S, Hayashi YK, Nishino I: Muscle from a 20-week-old myotubular myopathy fetus is not myotubular. Neuromuscular Disorders 2015.

[81] Helland IB, Smith L, Saarem K, Saugstad OD, Drevon CA: Maternal supplementation with very-long-chain n-3 fatty acids during pregnancy and lactation augments children's IQ at 4 years of age. Pediatrics 2003, 111:e39-44.

794 **Figure Legends**

795

796 **Figure 1. Typical pathological features of HACD1-CNM in Labrador Retriever dogs.** Images
797 to the left show representative low magnification images of H&E-stained 10 µm cryosections from
798 biceps femoris muscle biopsy samples from a control adult 40 month old dog (A) and HACD1-
799 CNM affected dogs at 11 months old (D), 30 months old (G) and 14 years old (J). Note the
800 variability in myofiber size, and greater fibrosis and fat infiltration in the older CNM-affected
801 animals. M, at higher magnification, from a 30 month old affected dog where prominent
802 pathological features such as abnormal internal staining pattern, centralized nuclei and small
803 hypotrophic fibres are evident.
804 The middle column images show SDH histochemistry of 10 µm cryosections from biceps femoris
805 muscle biopsy samples from a control adult (B) and HACD1-CNM affected dogs at 11 months old
806 (E), 30 months old (H) and 14 years old (K). Note the loss of fiber-type chequer-board pattern and
807 abnormal pattern of oxidative staining. Higher magnification image (N) is from an 11 month old
808 CNM-affected dog and shows numerous myofibers with the halo pattern (white arrowhead) that
809 was a common feature.
810 Images to the right are low magnification muscle ultrastructure showing representative features in
811 affected dogs at 11 months old (F), 30 months old (I) and 14 years old (L) in comparison with a
812 control adult dog (C). Normal myonuclei (indicated by asterisks *) are peripherally located (C)
813 whereas in HACD1-CNM-affected dogs, abnormal internalization can be seen. These were often
814 associated with clumps of mitochondria and, particularly in older dogs, clumps of dark staining
815 amorphous material (lipid bodies). Also notable in the 30 month old dog (I) is an area of focal
816 disorganization at the myofiber periphery, in addition internalized myonuclei can be seen in a
817 chain (asterisks). Scale bars represent 100 µm (A, D, G, J), 50 µm (B, E, H, K), 10 µm (M, N, I) or
818 1 µm (C, F, L).

819

820 **Figure 2. Triad abnormalities in dogs with canine HACD1-CNM.** (A-D) Electron micrographs
821 from longitudinal biceps femoris muscle sections showing t-tubule appearance from normal canine
822 muscle (17 month old dog, (A)) and affected dogs at 11 months old (B), 30 months old (C) and 14
823 years old (D). Inset images show selected representative single t-tubules in more detail. Note the
824 narrow, elliptical t-tubules in the normal dog, whereas in dogs with HACD1-CNM, t-tubules appear
825 more rounded and more dilated as they age. The inset image in C shows a t-tubule with

membranous contents. Scale bar represents 1 μm for main images, 0.5 μm for insets. Graphs show results of objective measurements of t-tubule morphometry performed from >125 t-tubules per dog from at least 5 myofibers: circularity (E) and area (F) are depicted in bar graphs showing mean of medians +/- S.D. A mixed effect model was used to assess significance – in comparison with control dogs, circularity was increased in affected dogs at both time points; and area was significantly increased at the later time point (*** P<0.001). Supplemental figure 1 shows these results in detail with all data points plotted for each dog.

Figure 3. Triad immunohistochemistry. Confocal images of transverse sections stained for DHPR and RyR1 (A-C) and BIN1 and RyR1 (D-F). High magnification images of representative myofibers from 17 month old control (A,D), 11 month old CNM (B,E) and 30 month old CNM (C,F) canine muscle. Note the regular "honey comb" pattern of the staining that outlines the bundles of myofilaments in the normal dog that is disrupted in the affected dogs with loss of this pattern and reduced staining intensity, particularly in the fiber periphery. In the older affected dog this becomes more prominent with more general disorganization and focal areas of dense staining. DHPR and RyR appear to colocalize variably across the fiber. Confocal images of longitudinal cryosections of biceps femoris muscle from 40 month old control (G, I) and 11 month old CNM-affected (H, J) dogs stained for BIN1 (G,H) and DHPR (I,J). Note the accumulations of these t-tubule associated proteins that extend from internalized nuclei (arrowheads). Bars represent 10 μm.

(K and L) Transmission electron micrograph images of transverse sections showing membranous structures of suspected tubuloreticular origin in 30 month old CNM affected dogs. The images show varying configurations including a subsarcolemmal rim of vesicular structures and mitochondria (K) and disorganization with mitochondria and tubular and vesicular membranes with a radial alignment towards the sarcolemma (L). Scale bars represent 1 μm.

Figure 4. Disorganized tubuloreticular membranes and mitochondria mislocalization. (A-I) Serial biceps femoris muscle cryosections from an 11 month old CNM affected dog stained with H&E (A), Gomori trichrome (GT) (B), BIN1 immunohistochemistry (C), oxidative stains (SDH (D), COX (E) and NADH-TR (F)) and dual labeling for RyR1 (G) and SERCA2 (H) merged with DAPI (I). These serial sections demonstrate that disorganization of tubuloreticular membranes (C, G, H) corresponds with the appearance of peripheral fiber oxidative halos (D, E, F). Note SERCA2

858 preferentially stains longitudinal SR in type I myofibers therefore the type 2 fibers (which are
859 reduced in number in HACD1-CNM affected dogs) are stained with RyR1 alone and appear red in
860 the merged image (I). Bar represents 50 μm. Representative control images for comparison can
861 be viewed in other figures as follows: H&E and SDH oxidative staining (figure 1), RyR1, DHPR
862 and BIN1 (figure 3).
863
864 **Figure 5. Sarcolemmal and internal membranous abnormalities with dysferlin**
865 **mislocalization.** Transverse (A and B) and longitudinal (C and D) electron micrographs from 30
866 month old HACD1-CNM affected dogs showing aberrant tubular and vesicular membranous
867 structures including sarcolemmal membrane invaginations (white arrow) and subsarcolemmal
868 vacuoles and caveolae (black arrowheads). Scale bars represent 1 μm.
869 Dysferlin immunohistochemistry (green) merged with DAPI (blue) on transverse cryosections from
870 (E) control 17 month old; (F) 11 month old CNM; (I) 30 month old CNM with internal cytoplasmic
871 staining; (J) 30 month old CNM with internalized focal membranous staining. The box depicted in
872 the lower magnification image (G) shows the region magnified in image (F) which corresponds to a
873 serial section stained with dMHC (H) demonstrating that only a few fibers with diffuse cytoplasmic
874 staining for dysferlin were dMHC positive (presumably regenerating) fibers. Image (K) shows
875 dysferlin alone (from image J) alongside a serial section stained with dystrophin (L) demonstrating
876 that internal membranous elements co-stain with this sub-sarcolemmal protein (arrowheads).
877 Scale bars represent 50 μm.
878
879 **Figure 6. Cytoskeletal abnormalities.** (A-C) Ultrastructural z-line abnormalities on longitudinal
880 sections (LS): (A and B) Hazy and disorganized/smeared z-lines from 11 month old and 30 month
881 old HACD1-CNM affected dogs respectively; (C) Accumulations of z-line material (rods) in a 14
882 year old affected dog (these were also observed in 30 month old dogs). (D-F) Myofibrillar
883 disorganization on transverse sections (TS) from 11 month old (D) and 30 month old (E) CNM
884 affected dogs: intermyofibrillar spaces are widened and bundles of myofilaments disrupted with
885 accumulations of tubular membranes and glycogen. (F) Transverse myofiber section from a 14
886 year old dog showing the progression into old age including a “cap” of extensive disorganization.
887 Bars for electron micrographs represent 1 μm.
888 (G-L) Immunohistochemistry for desmin (G-I) and sarcomeric myosin (MF20) (J-L). (G,J) 17 month
889 old control, (H,K) 11 month old CNM and (I,L) 30 month old CNM dogs. Note the disorganization

of these intermediate filament and contractile apparatus proteins particularly around the nuclei in CNM-affected dogs. Bars represent 20 μm. Exposures are not the same for desmin in all dogs: affected dogs required shorter exposure times versus normal.

Figure 7. Morphology of control (A-C) and *Hacd1*-KD (knock down) (D-F) myotubes at 12 days of differentiation. Phase contrast (A, D) and wide field immunofluorescence (RyR1 (B, E, magnified in insets)) and BIN1 (C, F)) images showing the typical appearance of differentiated myotubes from both cell lines. Note the presence of intracellular vesicles (D) and rings of abnormally positioned nuclei (E, F) in the knockdown cell line. Scale bars represent 50 μm.

Feature	Ctl5	Ctl6	CNM1	CNM2	CNM1-2	CNM2-2	Het2	CNM5
Objective counts								
H&E - centralized nuclei % over absolute count	0.8 6/785	0.4 3/814	14.0 84/601	15.6 122/781	38.5 328/851	51.7 429/829	1.7 13/771	43.2 389/511
SDH - abnormal pattern % over absolute count	0.3 1/385	0.9 3/331	78.0 199/255	81.5 296/363	85.2 225/264	86.6 219/253	7.1 22/308	90.3 261/289
SDH - “halo” pattern % over absolute count	0 0/385	0 0/331	50.6 129/255	51.0 185/363	16.7 44/264	22.1 56/253	0 0/308	6.9 20/289
Subjective scoring - H&E								
Centralized nuclei	0	0	+	+	++	++	0/+	++
Variable myofiber size	0	0	++	+++	++	+++	+	+++
Abnormal internal staining pattern	0	0	++	++	++/+++	+++	0/+	++/+++
Fatty infiltration/myofiber replacement	0	0	0/+	0/+	++/+++	++	0/+	+++
Fibrosis	0	0	0	0/+	++	++	0/+	+++
Subjective scoring - Trichrome								
Abnormal internal staining pattern	0	0	++/+++	+++	+++	+++	+	+++
Fibrosis	0	0	0/+	0/+	++	++	+	+++
Subjective scoring - Oxidative stains								
COX - abnormal pattern	0	0	++	+++	++/+++	+++	0	+++
NADH - abnormal pattern	0	0	++/+++	+++	+++	+++	0/+	+++
SDH - abnormal pattern	0	0	++	++/+++	+++	+++	0/+	+++
SDH - “halo” pattern	0	0	+/++	++	+	+/++	0	+
Subjective scoring - Other								
Oil red O - fat	0	0	+/0	+/++	++/+++	++	+	+++
Acid phosphatase positive staining	0	0	0	0	0	0	0	0

Table 1: Severity and progression of pathological features in dogs with HACD1-CNM at different ages. Summary of pathological features as derived from blinded evaluation of stained cryosections from each dog. Objective counts were performed to determine the percentage of fibers with centralized nuclei and abnormal oxidative staining pattern from random images of H&E

926 and SDH stained cryosections respectively. The lower section of the table displays results from
927 subjective scoring of other features as defined in the legend below - a range is given where the
928 feature varied across the section.
929 Legend:
930 0 within normal limits or feature absent
931 + mild (on subjective evaluation this feature is apparent but less than a third of fibers or of the field
932 of view is affected)
933 ++ moderate (around half of all fibers or of the field of view is affected)
934 +++ severe (greater than two thirds of fibers or of the field of view is affected)
935

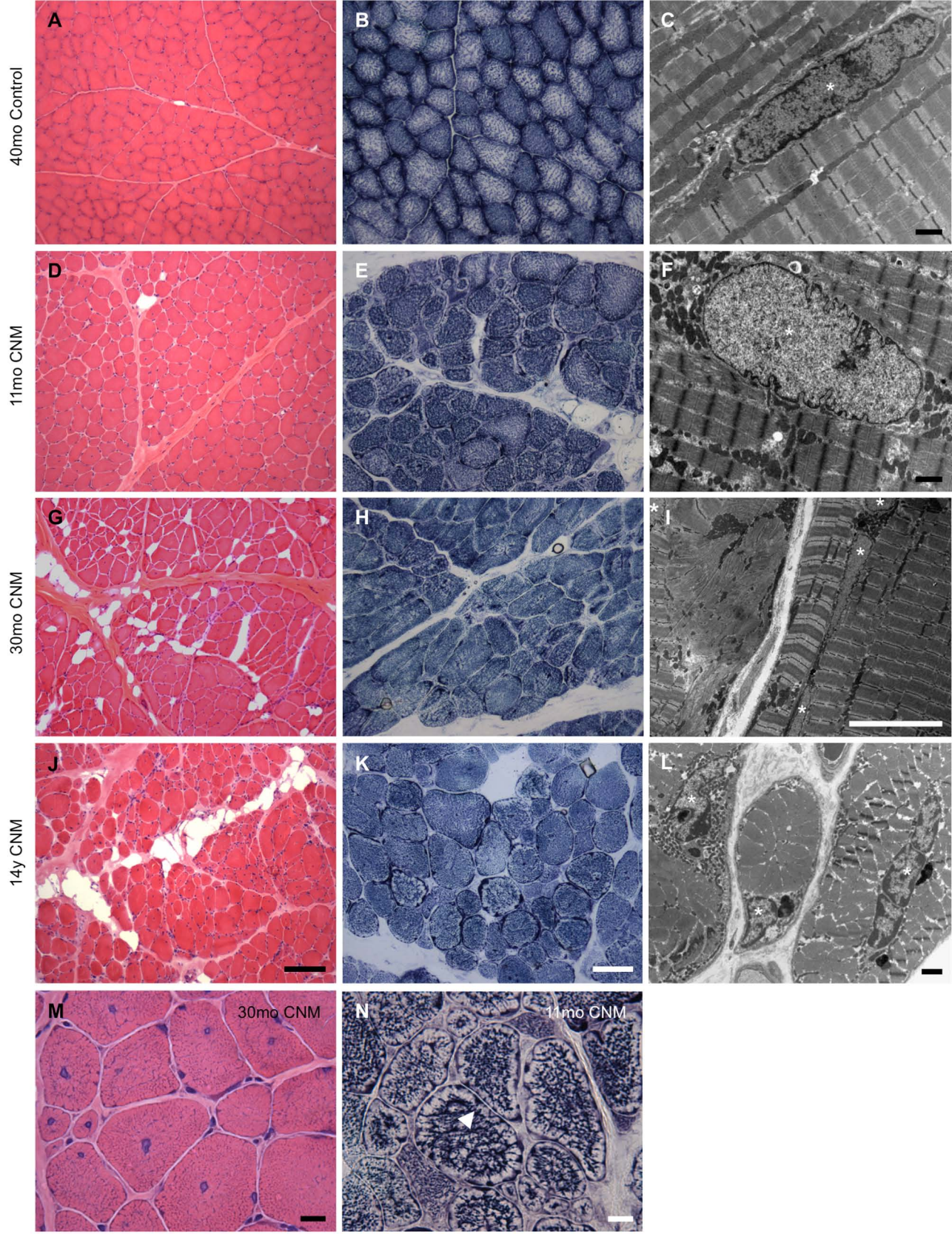
40mo Control
11mo CNM
30mo CNM
14y CNM
A
B
C
D
E
F
G
H
I
J
K
L
M
30mo CNM
N
11mo CNM

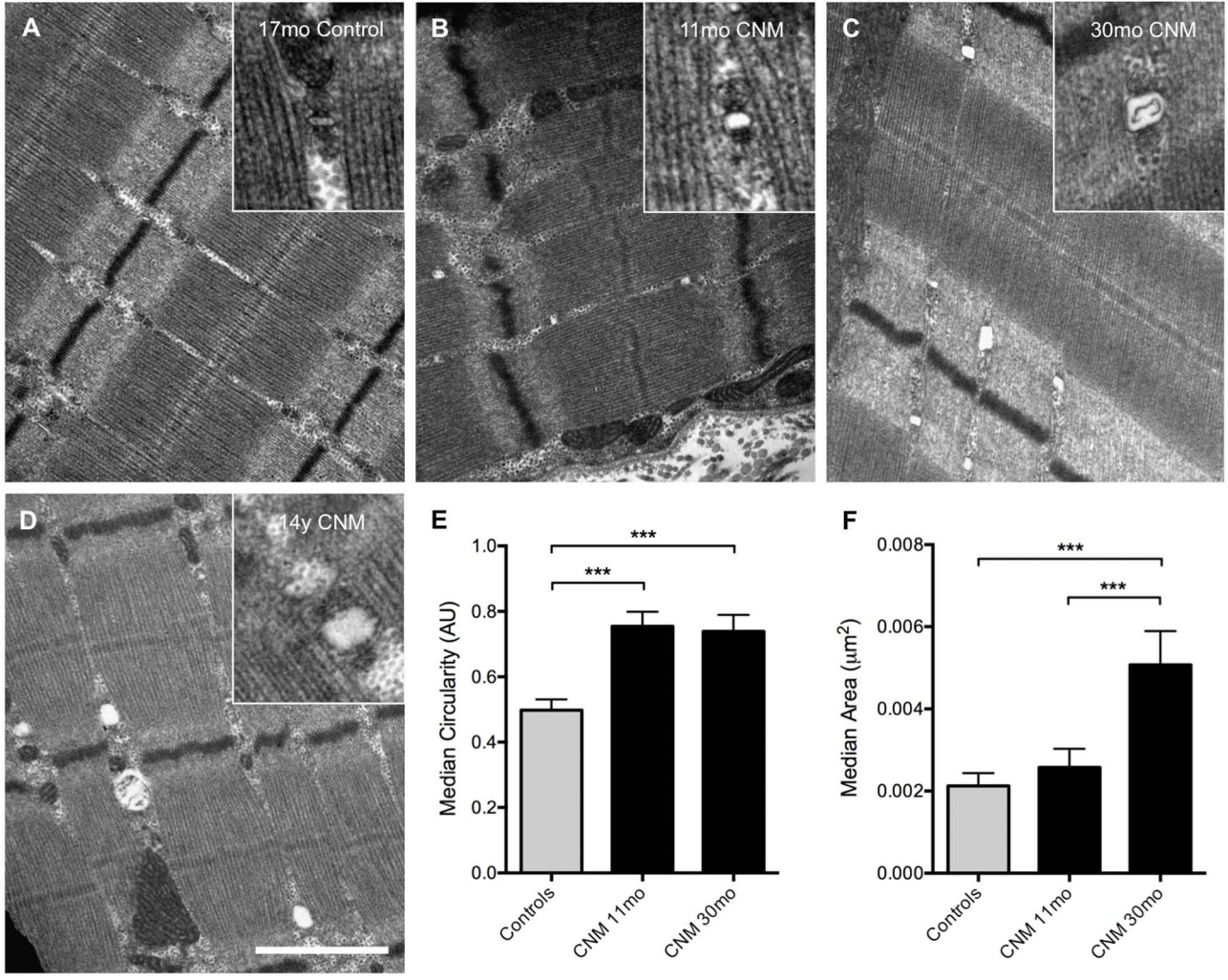
A
17mo Control
B
11mo CNM
C
30mo CNM
D
14y CNM
E
Median Circularity (AU)
1.0
0.8
0.6
0.4
0.2
0.0
***
***
Controls
CNM 11mo
CNM 30mo
F
Median Area (μm²)
0.008
0.006
0.004
0.002
0.000
***
***
Controls
CNM 11mo
CNM 30mo

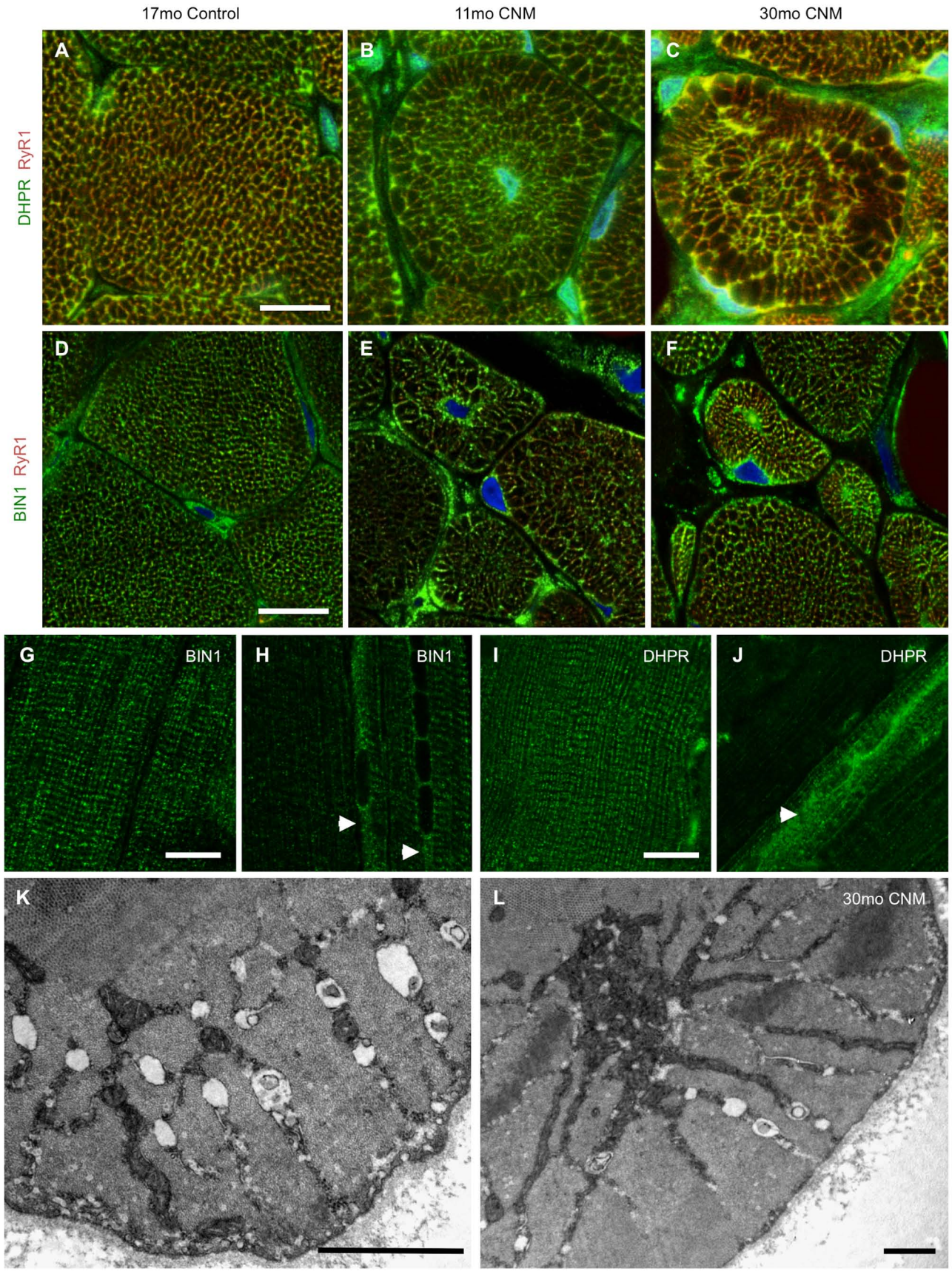
17mo Control
11mo CNM
30mo CNM
A
B
C
DHPR RyR1
D
E
F
BIN1 RyR1
G
BIN1
H
BIN1
I
DHPR
J
DHPR
K
L
30mo CNM

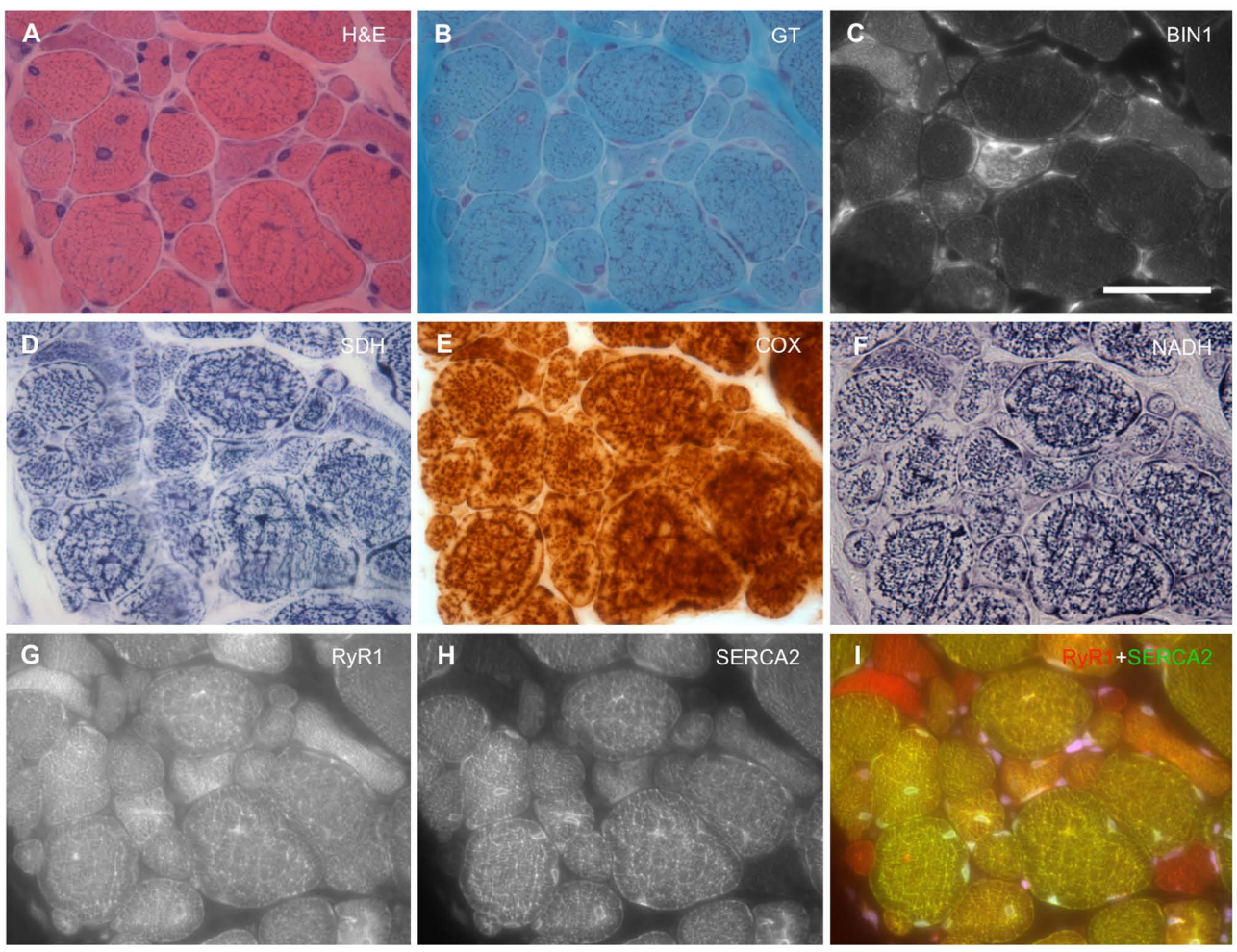
A
H&E
B
GT
C
BIN1
D
SDH
E
COX
F
NADH
G
RyR1
H
SERCA2
I
RyR1+SERCA2

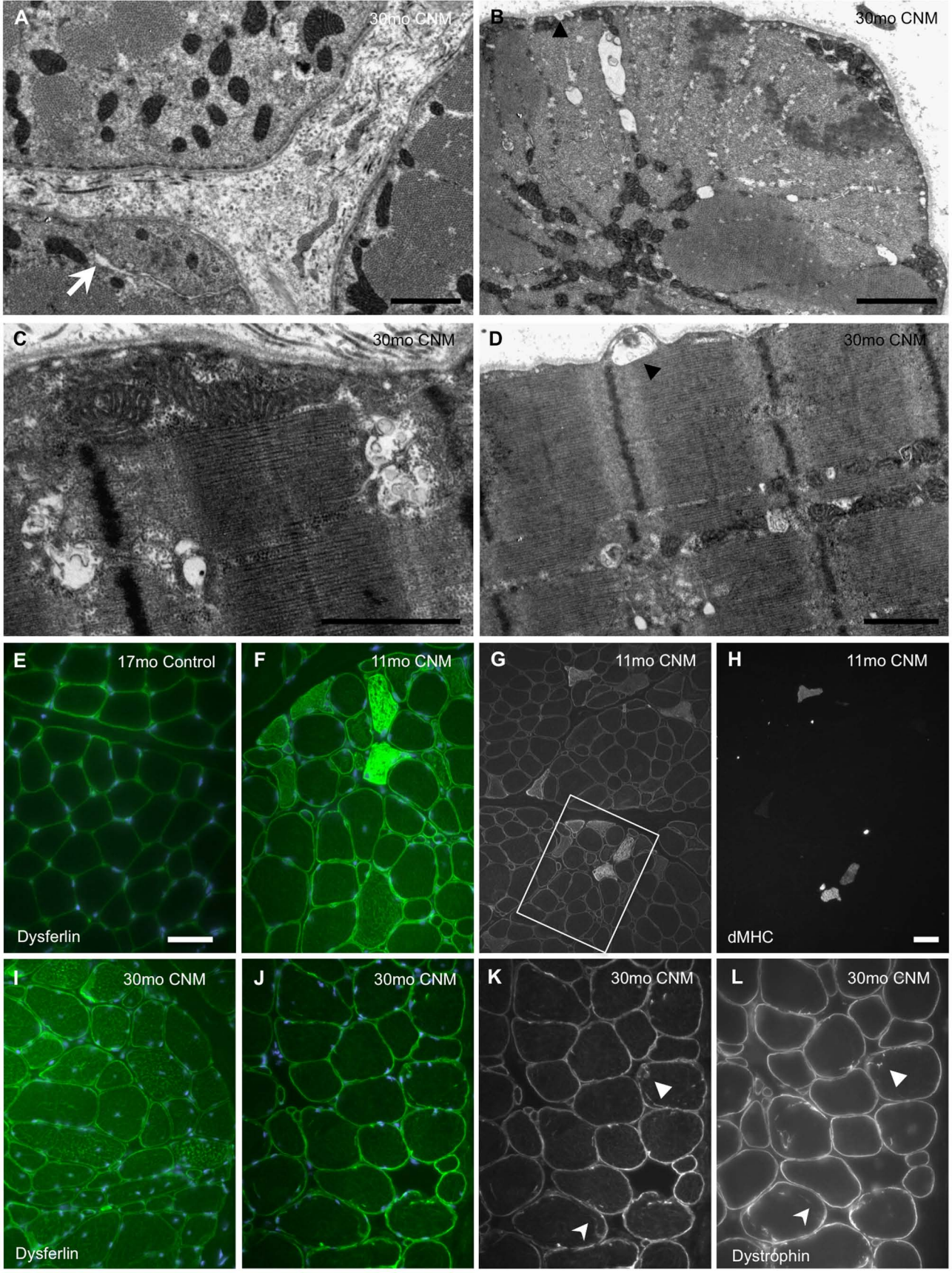
A
30mo CNM
B
30mo CNM
C
30mo CNM
D
30mo CNM
E
17mo Control
Dysferlin
F
11mo CNM
G
11mo CNM
H
11mo CNM
dMHC
I
30mo CNM
Dysferlin
J
30mo CNM
K
30mo CNM
L
30mo CNM
Dystrophin

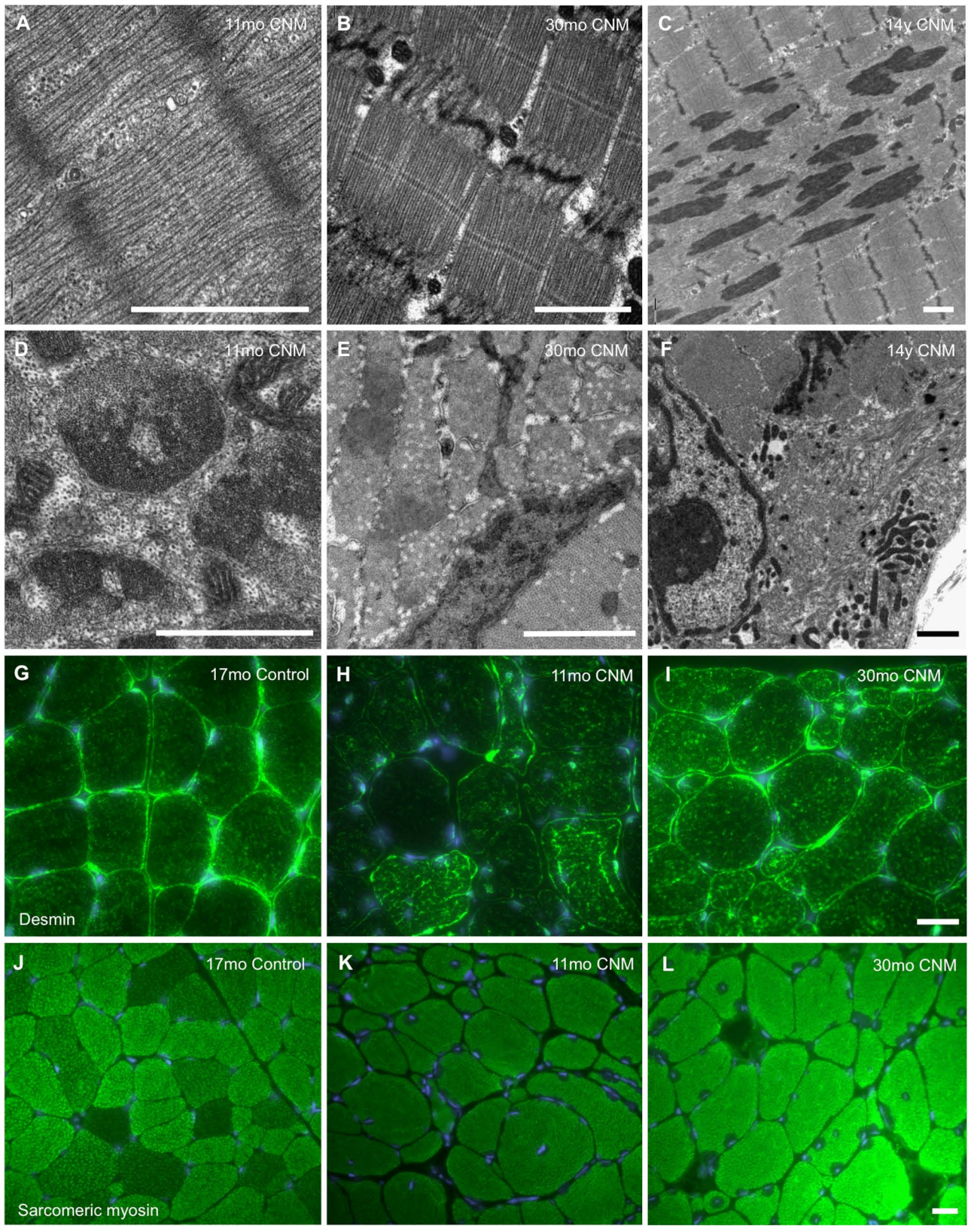
A
11mo CNM
B
30mo CNM
C
14y CNM
D
11mo CNM
E
30mo CNM
F
14y CNM
G
17mo Control
Desmin
H
11mo CNM
I
30mo CNM
J
17mo Control
Sarcomeric myosin
K
11mo CNM
L
30mo CNM

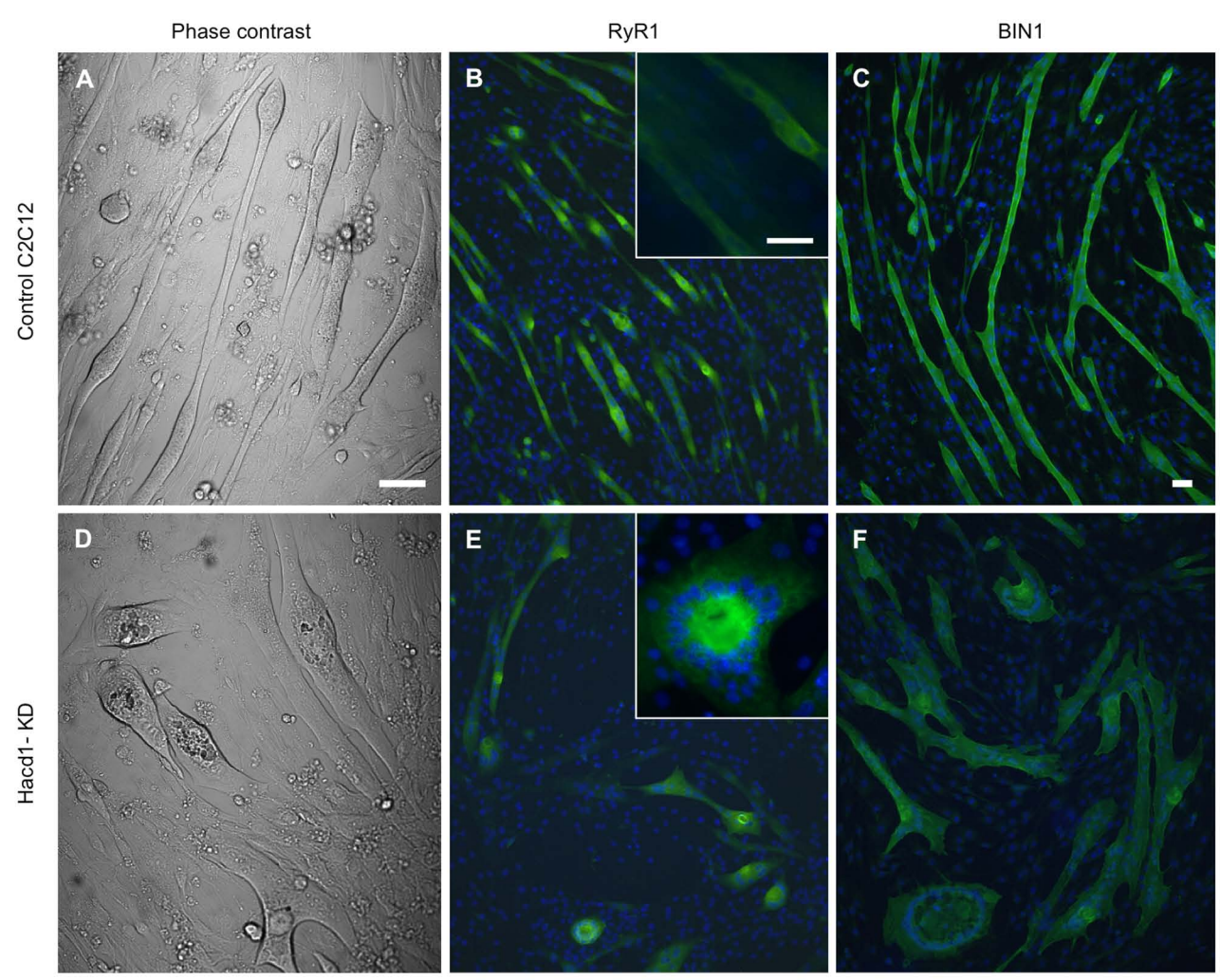
Phase contrast
RyR1
BIN1
Control C2C12
Hacd1- KD
A
B
C
D
E
F